Water Research

Geochemistry, stable isotopes and statistic tools to estimate threshold and source of nitrate in groundwater (Sardinia, Italy)

--Manuscript Draft--

Manuscript Number:	
Article Type:	Research Paper
Keywords:	Groundwater; nitrate pollution; stable isotopes; mixing models; Sardinia
Corresponding Author:	Elisabetta Dore University of Cagliari Monserrato, Cagliari, Sardinia ITALY
First Author:	Riccardo Biddau
Order of Authors:	Riccardo Biddau
	Elisabetta Dore
	Stefania Da Pelo
	Mario Lorrai
	Paolo Botti
	Maurizio Testa
	Rosa Cidu
Abstract:	In the European Union, nitrate vulnerable zone (NVZ) should be designed for the mitigation of nitrate (NO_3^-) contamination caused by agricultural practices. Before establishing new NVZ, the sources of NO_3^- must be recognized. A geochemical and multiple stable isotopes approach (hydrogen, oxygen, nitrogen, sulfur and boron) and statistical tools were applied to define the geochemical characteristics of groundwater (60 samples), calculate the local NO_3^- threshold and assess potential sources of NO_3^- contamination in two study areas (hereafter Northern and Southern), located in a Mediterranean environment (Sardinia, Italy). Hydrogeochemical features in the two study areas were similar: near neutral to slightly alkaline pH, electrical conductivity in the range of 0.3 to 3.9 mS/cm, and chemical composition ranging from Ca-HCO_3^- at low salinity to Na-Cl^- at high salinity. Some groundwater samples were distinguished by relatively high SiO_2 (up to 34 mg/L) and F^- (up to 2.6 mg/L). Concentrations of NO_3^- in groundwater were in the range of 1 to 165 mg/L (median value 30 mg/L), whereas the nitrogen reduced species were negligible, except few samples having NH_4^+ up to 2 mg/L. Threshold values (calculated by the mean + 2 times the standard deviation) in the studied groundwater samples were between 4 and 7 mg/L NO_3^-, which was in agreement with previous estimates in Sardinian groundwater. Values of δ^2H and $\delta^{18}O$ in groundwater indicated a meteoric origin with negligible fractionation processes since infiltration, and few exceptions. A group of samples collected in the Southern area was distinguished by a marked negative $\delta^{18}O$ shift, indicating oxygen isotopic exchange between the groundwater and the gas CO_2. Values of $\delta^{34}S$ and $\delta^{18}O$ SO_4 of SO_4^{2-} in groundwater samples indicated different sources of SO_4^{2-}. Sulfur isotopic features attributed to marine SO_4^{2-} were consistent with groundwater circulation in marine-derived sediments. Other source of SO_4^{2-} were recognize due to the oxidation of sulfide minerals, to fertilizers, manure, sewage fields, and SO_4^{2-} derived from a mix of different sources. Values of $\delta^{15}N$ and $\delta^{18}O$ NO_3 of NO_3^- in groundwater samples indicated different biogeochemical processes and NO_3^- sources. Nitrification and volatilization processes might have occurred at very few sites, and denitrification was likely to occur at specific sites. Mixing among various NO_3^- sources in different proportions might account for the observed NO_3^- concentrations and the nitrogen isotopic compositions. The SIAR modeling results showed a prevalent NO_3^- source from sewage/manure. The $\delta^{11}B$ signatures in groundwater indicated the manure to be the predominant NO_3^- source, whereas NO_3^- from sewage was recognized

	at few sites. Geographic areas showing either a predominant process or a defined NO_3^- source where not recognize in the studied groundwater. Results indicate widespread contamination of NO_3^- in the cultivated plain of both areas. Point sources of contamination, due to agricultural practices and/or inadequate management of livestock and urban wastes, were likely to occur at specific sites.
Suggested Reviewers:	Maddalena Pennisi maddalena.pennisi@igg.cnr.it expert in boron isotopes
	Roger Puig rpuig@ub.edu expert in nitrate geochemistry and isotopes
	Richard B. Wanty rwanty@mines.edu expert in geochemistry and baseline studies
	Enrico Dinelli enrico.dinelli@unibo.it expert in baseline studies, geochemistry and statistics

Dear Editor,

The manuscript “Geochemistry, stable isotopes and statistic tools to estimate threshold and source of nitrate in groundwater (Sardinia, Italy)”, by Riccardo Biddau, Elisabetta Dore, Stefania Da Pelo, Mario Lorrai, Paolo Botti, Maurizio Testa and Rosa Cidu is submitted for publication in Water Research.
Using the example of two study areas in Sardinia (Italy), this paper highlights the strength of an integrated study, combining hydrogeochemistry, multi-isotope techniques, statistic and GIS, for assessing nitrate source in groundwater. The topic here addressed is timely for accomplishing present regulations in Italy and European Union and establish adequate plans for reducing nitrate contamination in groundwater bodies.
This is an original manuscript that it is not under consideration for publication elsewhere, and its publication is approved by all authors. Authors thank the Editor of Water Research for considering publication of this paper.

Best regards,

D.ssa Elisabetta Dore
Università degli Studi di Cagliari (Italy)
Dipartimento di Scienze Chimiche e Geologiche
Blocco A, Cittadella Universitaria, 09042 Monserrato (Italy)
Tel. (+39) 070 67577
E-mail: elisabetta.dore@unica.it

Highlights

Geochemistry, multiple stable isotopes approach (hydrogen, oxygen, nitrogen, sulfur and boron) and statistical tools were applied to define the geochemical characteristics of groundwater, calculate the local nitrate threshold and assess potential sources of nitrate.

Mixing model results showed a prevalent nitrate source from sewage and/or manure. The boron isotopic signatures in groundwater indicated the manure to be the predominant source. Nitrification and volatilization processes might have occurred at few sites and denitrification was likely to occur at specific sites.

Declaration of interests

☒The authors declare that they have no known competing financial interests or personal relationships that could have appeared to influence the work reported in this paper.

☐The authors declare the following financial interests/personal relationships which may be considered as potential competing interests:

Geochemistry, stable isotopes and statistic tools to estimate threshold and source of nitrate in groundwater (Sardinia, Italy)

Riccardo Biddau[a], Elisabetta Dore[a*], Stefania Da Pelo[a], Mario Lorrai[b], Paolo Botti[b], Maurizio Testa[c], Rosa Cidu[a]

[a] Department of Chemical and Geological Sciences, University of Cagliari, Blocco A - Monserrato, Italy
[b] Regione Autonoma della Sardegna-ADIS-Servizio tutela e gestione delle risorse idriche, via Mameli 88, 09100 Cagliari, Italy
[c] Agenzia Regionale per la Protezione dell'Ambiente della Sardegna - Servizio Controlli, Monitoraggi e Valutazione Ambientale della Direzione Tecnico Scientifica, via Carloforte, 09100 Cagliari, Italy

[*] Corresponding Author email: elisabetta.dore@unica.it

Keywords
Groundwater, nitrate pollution, stable isotopes, mixing models, Sardinia

Abstract
In the European Union, nitrate vulnerable zone (NVZ) should be designed for the mitigation of nitrate (NO_3^-) contamination caused by agricultural practices. Before establishing new NVZ, the sources of NO_3^- must be recognized. A geochemical and multiple stable isotopes approach (hydrogen, oxygen, nitrogen, sulfur and boron) and statistical tools were applied to define the geochemical characteristics of groundwater (60 samples), calculate the local NO_3^- threshold and assess potential sources of NO_3^- contamination in two study areas (hereafter Northern and Southern), located in a Mediterranean environment (Sardinia, Italy).
Hydrogeochemical features in the two study areas were similar: near neutral to slightly alkaline pH, electrical conductivity in the range of 0.3 to 3.9 mS/cm, and chemical composition ranging from Ca-HCO_3^- at low salinity to Na-Cl^- at high salinity. Some groundwater samples were distinguished by relatively high SiO_2 (up to 34 mg/L) and F^- (up to 2.6 mg/L). Concentrations of NO_3^- in groundwater were in the range of 1 to 165 mg/L (median value 30 mg/L), whereas the nitrogen reduced species were negligible, except few samples having NH_4^+ up to 2 mg/L. Threshold values (calculated by the mean + 2 times the standard deviation) in the studied groundwater samples were between 4 and 7 mg/L NO_3^-, which was in agreement with previous estimates in Sardinian groundwater.
Values of δ^2H and $\delta^{18}O$ in groundwater indicated a meteoric origin with negligible fractionation processes since infiltration, and few exceptions. A group of samples collected in the Southern area was distinguished by a marked negative $\delta^{18}O$ shift, indicating oxygen isotopic exchange between the groundwater and the gas CO_2. Values of $\delta^{34}S$ and $\delta^{18}O_{SO4}$ of SO_4^{2-} in groundwater samples indicated different sources of SO_4^{2-}. Sulfur isotopic features attributed to marine SO_4^{2-} were consistent with groundwater circulation in marine-derived sediments. Other source of SO_4^{2-} were recognize due to the oxidation of sulfide minerals, to fertilizers, manure, sewage fields, and SO_4^{2-} derived from a mix of different sources.
Values of $\delta^{15}N$ and $\delta^{18}O_{NO3}$ of NO_3^- in groundwater samples indicated different biogeochemical processes and NO_3^- sources. Nitrification and volatilization processes might have occurred at very few sites, and denitrification was likely to occur at specific sites. Mixing among various NO_3^- sources in different proportions might account for the observed NO_3^- concentrations and the nitrogen isotopic compositions. The SIAR modeling results showed a prevalent NO_3^- source from sewage/manure. The $\delta^{11}B$ signatures in groundwater indicated the manure to be the predominant NO_3^- source, whereas NO_3^- from sewage was recognized at few sites. Geographic areas showing either a predominant process or a defined NO_3^- source where not recognize in the studied groundwater. Results indicate widespread contamination of NO_3^- in the cultivated plain of both areas. Point sources of contamination, due to agricultural practices and/or inadequate management of livestock and urban wastes, were likely to occur at specific sites.

1. Introduction

Large amounts of water resources of the world are affected by nitrate pollution that negatively impacts on human health and ecosystems. Natural waters may contain different nitrogen species, i.e. dissolved gas from

the atmosphere (N_2), ammonia (NH_3) from rain and soil, the ions ammonium (NH_4^+), nitrite (NO_2^-) and nitrate (NO_3^-), and organic nitrogen compounds (Stumm and Morgan, 1996). Sources of nitrogen ions include the soil, fertilizers, sewage, manure, industrial effluents, and geologic materials containing soluble nitrogen compounds. Nitrate is the end product of nitrification processes, and is usually taken up by plants. The excess NO_3^- goes into water systems because it is poorly absorbed by clay minerals and is stable in aqueous media unless denitrification processes occur. The NO_3^- stability in solution under a wide range of pH and redox conditions, may result in concentrations above the guideline of 50 mg/L established by the World Health organization (WHO, 2011), which are frequently observed in water systems, including drinking water (Sarkar et al., 2021; Picetti et al., 2022).

Since the 1991, the European Commission has promoted specific measures aimed to minimize NO_3^- contamination derived from agricultural practices (Nitrate Directive – EC, 1991). Nevertheless, data collected until the 2019 in the European State Members showed that 14.1% of groundwater stations still exceeded 50 mg/L NO_3^- in annual average and that there has been no overall decrease of NO_3^- concentration in groundwater in the last 20 years (EC, 2021). This suggests that further measures should be taken to mitigate groundwater contamination by NO_3^-. Before establishing new rules for contaminated areas, the sources of NO_3^- must be recognized.

Different approaches have been used to track NO_3^- sources in groundwater: the water chemistry, isotopic signatures, microbial composition, statistics, and combinations of them (Menció et al., 2016; Kazakis et al., 2020; Cao et al., 2022). In particular, due to the peculiar isotopic signatures of different sources, multiple stable isotopes (Yu et al., 2020; Carrey et al., 2021; Ryu et al., 2021; He et al., 2022) and statistical models (i.e.: Bayesian SIAR model, Parnell et al., 2013; Meghdadi and Javar, 2018; Ren et al., 2022) has been used to quantify the relative contributions of potential NO_3^- sources.

In Sardinia (Italy), the intensive dairy cattle district of Arborea has been declared a nitrate vulnerable zone (NVZ) in 2005, and a specific Action program for the reduction of NO_3^- has been developed (Biddau et al., 2019). However, other well in Sardinia than those located within the Arborea NVZ, showed NO_3^- concentrations above 50 mg/L that persisted several years, thus demanding targeted actions to reduce the contamination. According to the Nitrate Directive (EC, 2006), the European Member States are required to identify groundwater bodies (GWBs) at risk of failing to meet the environmental objectives, as well to designate as NVZ the areas being at risk from agricultural nitrate pollution. This study was aimed at investigating two areas to be eventually designated as new NVZ in Sardinia. To this purpose a combination of geochemical, isotopic and statistical tools were applied. Specific objectives were to: *i)* define the geochemical characteristics of groundwater samples; *ii)* calculate the local threshold of NO_3^- in groundwater; *iii)* investigate the behavior of deuterium, oxygen-18, nitrogen-15, sulfur-34 and boron-11 stable isotopes to recognize the potential sources of nitrate contamination.

2. Study areas

The areas selected for this investigation are located in the North and South Sardinia (Fig. 1). Climate is Mediterranean with warm dry summers and mild rainy winters. The mean annual temperature is 15.9 °C and mean annual precipitation is 537 mm, the latter mostly concentrated between October and March (Frau et al., 2020). Land uses consist of woodland, Mediterranean maquis, orchards, olive groves, arable fields and natural grazing; greenhouses are mostly located in the South (RAS, 2013b). Industrial activities (mainly chemistry and mechanics plants) occur at Porto Torres in the North, at Macchiareddu in the South, and nearby the towns of Cagliari and Sassari (Fig. 1).

Main geological features of Sardinia consist of a segment of the western European Variscan metamorphic basement, covered by continental Upper Carboniferous–Permian sedimentary and volcanic deposits, Mesozoic carbonatic shelf sediments, Tertiary to Quaternary volcanic and sedimentary sequences (Sinisi et al., 2012).

Geological features in the Northern zone are comprised of the Paleozoic basement, the Mesozoic cover and Tertiary to Quaternary volcanic and sedimentary sequences. Shallow marine sedimentation with evaporite and carbonate occurred from the Middle Triassic to the Middle Cretaceous; the shelf sea covered the entire post-Variscan peneplain of Sardinia in the Middle Jurassic (Mameli et al., 2007). From the Oligocene to Middle Miocene, volcanic activity produced calc-alkaline sequences, ranging from basaltic to rhyolitic in composition (Sinisi et al., 2012). After the rotation of the Sardinia–Corsica block, a widespread transgression took place, with a system of shallow half-graben filled up by carbonatic and siliciclastic sequences of Upper Burdigalian–Tortonian age (Funedda et al., 2000). The Miocene sequence is made up of marl sandstone, siltstone, limestone and conglomerate. Geological sequences also include basaltic rocks of Pliocene-Pleistocene age and Quaternary deposits.

The Southern zone is located in the southernmost portion of the Campidano, namely the Graben of Cagliari. Geology mainly consists of Quaternary deposits related to the subsiding cycle of the Middle Pliocene. The Graben of Cagliari was filled up by sand, mud, conglomerate, lacustrine clay and, more recently, by fluvial deposits (Angelone et al. 2005, and references therein). Extensional tectonics affected the Graben of Cagliari during Pliocene-Pleistocene time, with NW-SE oriented faults (Cocco et al., 2012; 2013). A relevant industrial area (about 9000 ha) is included in the Southern area, which includes chemical and petro-chemical plants, port activities, refineries and incinerators (Frontalini et al., 2009).

According to the requirements of the European Water Framework Directive (EC, 2000), thirty-eight main hydrogeologic complexes were recognized in Sardinia. They are constituted of one or more hydrogeologic units, with homogenous lithology and degree of permeability and are divided in 114 GWBs. The investigated GWBs are hosted in Pliocene-Quaternary sediments (CIS 0511, 0121, 1721, 1722), in Oligocene-Miocene detritus-carbonatic sediments (CIS 2311, 2312, 2321) and in Mesozoic carbonatic rocks (CIS 3211), with locations and main groundwater flow directions shown in Figure 1.

3. Sampling and methods

The sampling strategy was aimed at recognizing the GWBs subjected to agricultural and livestock pressures, based on data acquired in the framework of the groundwater monitoring program established by the Sardinian Region. In particular, GWBs where wells contained a concentration higher than 50 mg/L of NO_3^-, GWB exposed to relevant industrial pressure, and groundwater wells used for drinking water, were selected to carry out hydrogeochemical surveys. Groundwater samples submitted to both chemical and isotopic analyses consisted of 7 springs and 53 wells; 29 samples were located in the Northern area and 31 in the Southern area. To characterize the potential source of contamination, 10 samples were collected at urban wastewater treatment plants, which inputs comprised a mix of sewage and run-off rain water in variable proportions according with seasonality. Other 56 groundwater samples, located in the Northern (20 samples) and Southern (36 samples) area, were considered for the calculation of NO_3^- threshold values in each area. The location of water samples in the two study areas is shown in Figure 1.

In situ, the water table level of wells, flow of springs, temperature, pH, electrical conductivity (EC) and dissolved oxygen were measured. Each well was purged before the collection of water. Immediately upon collection, the water was filtered through 0.22 μm pore-size filters in pre-cleaned high-density PE bottles and keep cooled by a portable refrigerator. One aliquot was acidified immediately upon filtration to 1% (v/v) HNO_3 supra pure. Aliquots for the nitrate isotope analyses were frozen in situ in order to prevent any alteration due to biological processes.

Analysis of major ions, nitrogen species and Mn were carried out within the framework of the R.A.S. groundwater-monitoring program at certified laboratories (RAS, 2011).

Boron and Si were determined at the University of Cagliari by inductively coupled plasma mass spectrometry (ICP-MS) and inductively coupled plasma optical emission spectrometry (ICP-OES). For each analytical run, the detection limits (DL) were calculated at 5 times the standard deviation (SD) plus the mean value calculated on several analyses of the blank solution. The standard reference solutions SRM1643d,e (supplied by the US National Institute of Standard & Technology, Gaithersburg, Maryland) and EnviroMAT ES-L-3 (supplied by SCP Science, St. Laurent, Quebec) were used to estimate analytical errors, which were usually below 5 %.

With reference to the evaluation of groundwater quality, the guidelines established by the WHO (2011) for drinking water and threshold values established by Italian legislations for drinking water and for the protection of groundwater (GURI, 2006; 2009; 2016) were considered. It is worth remembering that the Italian legislation incorporates the European legislation concerning the protection of groundwater against pollution and deterioration (EC, 2006; 2014).

The δ^2H and $\delta^{18}O$ of water ($\delta^{18}O_{H2O}$), $\delta^{15}N$ and $\delta^{18}O$ of dissolved NO_3^- ($\delta^{18}O_{NO3}$), $\delta^{34}S$ and $\delta^{18}O$ of dissolved SO_4^{2-} ($\delta^{18}O_{SO4}$), and $\delta^{11}B$ were determined. The δ^2H and $\delta^{18}O_{H2O}$ were measured using Wavelength-Scanned Cavity Ringdown Spectroscopy (L2120-i, Picarro). The $\delta^{15}N$ and $\delta^{18}O_{NO3}$ of NO_3^- were determined by Isotope Ratio Mass Spectrometer (IRMS, Finnigan MAT-253, Thermo Scientific). The $\delta^{34}S$ and $\delta^{18}O_{SO4}$ of SO_4^{2-} were determined by IRMS (Carlo Erba EA - Finnigan Delta C - ThermoQuest). Isotopic analyses of water, nitrate and sulfate were performed at the laboratory of the Mineralogia Aplicada i Medi Ambient, University of Barcelona, Spain, with details on analytical methods being reported in Puig et al. (2017). The $\delta^{11}B$ was determined by MC-ICP-SFMS at the Scandinavia ALS Laboratory Group, Sweden, with details on analytical methods being reported in Venturi et al. (2015). Isotopic results were expressed in terms of δ (Coplen, 2011) relative to the international standard Vienna Standard Mean Oceanic Water (V-SMOW) for δ^2H, $\delta^{18}O_{H2O}$, $\delta^{18}O_{NO3}$ and $\delta^{18}O_{SO4}$; the Vienna Canyon Diablo Troilite (V-CDT) for $\delta^{34}S$; the air for $\delta^{15}N$; and NBS951 for

$\delta^{11}B$. Analytical errors calculated using international and internal laboratory standards were (±δ‰): 1 $\delta^{2}H$, 0.15 $\delta^{18}O_{H2O}$, 1.0 $\delta^{18}O_{NO3}$, 0.5 $\delta^{18}O_{SO4}$, 0.6 $\delta^{15}N$, 0.2 $\delta^{34}S$ and 0.05 $\delta^{11}B$.

The observed NO_3^- concentrations in waters in the studied areas were fitted with a normal (Gaussian) mixture model (McLachlan and Peel, 2000) to recognize subgroups in the population of waters using the "MIXTOOLS" package (Benaglia et al., 2009) implemented in the R software, a free language for statistical computing (R Development Core Team, 2013). The maximum likelihood estimates of the parameters (mean and standard deviation, SD) with normal distributions for each subgroup was calculated using the expectation maximization (EM) algorithm (Dempster et al., 1977). The mean+2SD values of the population having the lowest NO_3^- concentrations was considered as the threshold value for nitrate in the studied areas, representing the present-day background concentrations of NO_3^- (Panno et al., 2006).

Nitrate produced by nitrification typically has a comparatively low $\delta^{18}O$ relative to atmospheric and fertilizer NO_3^-, which is assumed to derive from the fractional contribution of oxygen atoms originating from O_2 and water during the biological oxidation of NH_4^+ to NO_3^-, according to the following experimental equation (Andersson and Hooper, 1983):

(1) $\delta^{18}O_{NO3} = 2/3\ \delta^{18}O_{H2O} + 1/3\ \delta^{18}O_{O2}$

where $\delta^{18}O_{H2O}$ represents the measured value in the local groundwater samples and $\delta^{18}O_{O2}$ is the +23.5‰ value for atmospheric O_2 (Aravena and Mayer, 2010).

The relative contribution of the potential nitrate sources in groundwater samples were calculated using the Bayesian isotope mixing model in the SIAR package (Stable Isotope Analysis in R, Parnell et al., 2008). Dual-isotopic nitrate values ($\delta^{15}N$ and $\delta^{18}O$ of NO_3^-) and five potential local sources: NH_4 synthetic fertilizers (NH_4-fert.), NO_3^- fertilizers (NO_3-fert.), soil organic nitrogen (N-soil), sewage and manure (S-M) were included in the model. The isotopic compositions of selected end-members were assumed from the literature (Torres-Martinez et al., 2021) as follows: NH_4-fert.: $\delta^{15}N_{NO3}$ 1.24 ± 1.44‰, $\delta^{18}O_{NO3}$ 3.44 ± 2.47‰; NO_3-fert.: $\delta^{15}N_{NO3}$ -0.07 ± 2.85, $\delta^{18}O_{NO3}$ 24.12 ± 3.17‰; N-soil: $\delta^{15}N_{NO3}$ 3.26 ± 1.99‰, $\delta^{18}O_{NO3}$ 3.34 ± 2.04‰ and M-S: $\delta^{15}N_{NO3}$: 10.14 ± 4.53‰, $\delta^{18}O_{NO3}$ 5.69 ± 2.91‰.

Geochemical maps were drawn using ArcGIS 10.2 (ESRI, 2013).

4. Results and discussion

4.1 Hydrogeochemistry

Composition of host aquifers and recharge areas definitely influence the main geochemical characteristics of groundwater.

Physical and chemical features of groundwater in the Northern area are reported in Supplementary Material (SM) Table 1. Temperature ranged from 11 to 22 °C, with median value of 16 °C. The pH was near neutral to slightly alkaline (6.7 - 8.0). Values of EC and dissolved oxygen showed a large range, respectively from 0.7 to 4.0 µS/cm and from 3 to 9 mg/L (SM Table 1). The low salinity waters generally showed calcium-bicarbonate predominant composition, which was consistent with circulation of these waters in Tertiary and Mesozoic carbonate aquifers. At high salinity sodium-chloride composition prevailed, whereas magnesium and sulfate were relatively less abundant. Groundwater samples A35, A37, A41 showed predominant Na-bicarbonate composition (Fig. 2a piper). Concentrations of Na and Cl^- in groundwater followed the seawater dilution line, but few samples were slightly enriched in Na with respect to Cl^-, with Na likely derived from the weathering of Na-bearing feldspar. Concentrations of F^- were in the range of 0.05 to 0.8 mg/L (median 0.14 mg/L). Concentrations of Br^- were correlated with Cl^- ($R^2 = 0.941$). The NO_3^- concentrations were in the range of 4 to 165 mg/L, with the highest value showing the highest K concentration (SM Table 1). Reduced nitrogen species were undetectable in most samples; NO_2^- was only detected in 4 samples (up to 2.3 mg/L), and 3.6 mg/L NH_4^+ occurred at the outflow of sewage treatment plant (SM Table 1). Concentrations of SiO_2 ranged from 3 to 20 mg/L, median value of 7 mg/L, and were not related to temperature. Concentrations of B varied from 19 to 270 µg/L (median 74 µg/L), with values generally increasing with increasing Cl^- ($R^2 = 0.660$). Concentrations of B were not related to temperature, F^- and SiO_2.

Physical and chemical characteristics of groundwater in the Southern area are reported in SM Table 2. Temperature ranged from 13 to 24 °C. The pH was slightly acidic to alkaline (6.4 - 8.2). Values of EC and dissolved oxygen showed a large range, respectively from 0.3 to 3.9 µS/cm and from 2 to 9 mg/L (SM Table 2). The low salinity waters generally showed Ca-bicarbonate predominant composition; at high salinity the Na-chloride composition prevailed; magnesium and sulfate were relatively low, with the exception of

groundwater sample A61 showing a marked Ca-Mg-sulfate composition (Fig. 2b). Groundwater samples A3, A15, A56, A58 showed a predominant Na-bicarbonate composition (Fig. 2b). Concentrations of Na and Cl^- in groundwater showed molar ratios similar to seawater, with few samples slightly enriched in Na with respect to Cl^-. Concentrations of Br^- were correlated with Cl^- ($R^2 = 0.997$). Concentrations of F^- were in the range of 0.06 to 2.6 mg/L (median 0.17 mg/L). The NO_3^- concentrations were in the range of 1 to 83 mg/L. Reduced nitrogen species were undetectable in most samples, NO_2^- was always < 0.02 mg/L (SM Table 2), and up to 2 mg/L NH_4^+ occurred in six samples (SM Table 2). Silica ranged from 2 to 34 mg/L (SM Table 2), with a median value of 12 mg/L. The groundwater sample A18 having the highest SiO_2 concentration also showed relatively high concentrations of F^- (SM Table 2). Concentrations of B varied from 16 to 380 µg/L and were slightly correlated with Cl^- ($R^2 = 0.488$).

4.2 Nitrate distribution and threshold

Figure 3 shows cumulative distribution plots comparing NO_3^- concentrations in all groundwater samples collected in the studied areas. Median values of NO_3^- (about 30 mg/L) and the cumulative distributions were similar in both areas.

Figure 4 shows the statistical distribution of log-transformed NO_3^- concentrations for the Northern area (a) and Southern area (b). For each area, the NO_3^- threshold was calculated by the mean+2SD of the population showing the lower concentrations. The resulting threshold values were 7 and 4 mg/L NO_3^- in groundwater of the Northern and Southern area, respectively. These threshold values were in agreement with the NO_3^- threshold calculated for Sardinian groundwater hosted in granitic and metamorphic rocks (Biddau et al., 2017), and similar to present-day background values reported elsewhere (Kim et al., 2015; Carrey et al., 2021; Sarkar et al., 2021; Manu et al., 2022).

Figure 5 shows the spatial distribution and boxplot of NO_3^- concentrations in all groundwater samples within the two areas, together with a simplified land use map (modified after RAS, 2013b). In both areas, groundwater samples with NO_3^- concentrations above and below the threshold values was observed at the same locations, suggesting a probably point sources contamination of NO_3^-.

4.3 Isotopic composition of water

Results of deuterium and oxygen-18 isotopes determined in groundwater samples collected in the Northern area and Southern area are reported in SM Table 1 and SM Table 2, respectively.

Figure 6 shows the relationship between the δ^2H and $\delta^{18}O$ values in the studied groundwater samples. Most of samples lie close to the GMWL (Global Meteoric Water Line, Craig, 1961) and the IMWL (Italian Meteoric Water Line proposed for southern Italy, Giustini et al., 2016), indicating a meteoric origin of groundwater samples. Groundwater in the Northern area did not undergo significant isotopic fractionation since their infiltration. The groundwater A10 in the Southern area showed the less negative values of δD and $\delta^{18}O$, indicating evaporation; this interpretation is consistent with hydrogeological evidence showing lake water infiltration into this well. The groundwater samples A53 to A62 collected in the Southern area were distinguished by a marked negative $\delta^{18}O$ shift (Fig. 6b), likely indicating oxygen isotopic exchange between the groundwater and the gas phase CO_2. These samples were located in correspondence of faults bordering the Campidano graben (Cocco et al., 2012), where thermal waters occur (Angelone et al., 2005; Frau et al., 2020). Groundwater samples A56 and A58 showed water temperature of 23 and 24 °C, respectively, Na-bicarbonate-chloride composition (Fig. 2b), Ca/HCO_3^- molar ratio of 0.14 and 0.19, respectively, and A58 also showed the highest F^- (SM Table 2). These characteristics were similar to the CO_2-rich thermal waters of the Campidano, thus explaining the negative $\delta^{18}O$ shift observed in Figure 6b. However, a potential influence of industrial activities on the CO_2 flux in this area cannot be excluded and would needs further investigations.

4.4 Isotopic composition of sulfate

Results of sulfur-34 and oxygen-18 in SO_4^{2-} determined in groundwater samples collected in the Northern area and Southern area are reported in SM Table 1 and SM Table 2, respectively. Figure 7 shows values of $\delta^{18}O_{SO4}$ versus $\delta^{34}S$ of SO_4^{2-} in groundwater samples collected in the Northern (a) and Southern (b) areas, together with boxes of potential SO_4^{2-} sources (from Puig et al., 2017). The isotopic compositions indicated different sources of SO_4^{2-} in groundwater samples. Many samples showed isotopic features attributed to SO_4^{2-} derived from the interaction of water with marine sediments. These findings were consistent with the location of these samples in correspondence of marine sediments derived host aquifer. Groundwater samples A38 and A47 (Fig. 7a), and A62 (Fig. 7b) showed $\delta^{18}O_{SO4}$ versus $\delta^{34}S$ values attributed to SO_4^{2-} derived from the oxidation of sulfide minerals. The groundwater sample A61, having a high concentration of SO_4^{2-} (SM Table 2), showed a

sulfur isotopic signature attributed to fertilizers (Fig. 7b). Other samples were in the soil, manure, sewage fields, and still others might have isotopic signatures indicating SO_4^{2-} being derived from a mix of different sources. Groundwater samples A2, A10, A58, A20 in the Southern zone were characterized by relatively low concentrations of NO_3^- and SO_4^{2-} (SM Table 2), indicating a probably favorable condition to denitrification processes occur.

4.5 Nitrate source identification - multi-isotopic approach and SIAR model

Results of N-15 and O-18 in NO_3^- determined in groundwater samples collected in the Northern area and Southern area are reported in SM Table 1 and SM Table 2, respectively. Figure 8 shows values of $\delta^{15}N$ and $\delta^{18}O_{NO3}$ of nitrate in groundwater samples collected in the Northern (a) and Southern (b, c) areas.

According to the experimental equation proposed by Andersson and Hooper, 1983, the expected values of $\delta^{18}O_{NO3}$ derived from the nitrification of NH_4^+ should range between +3.2‰ and +4.3‰ in the Northern area ($\delta^{18}O_{H2O}$ range: -6.9 to -5.3‰, SM Table 1 and Fig. 8a), from +3.5‰ to +5.3‰ in the Southern area ($\delta^{18}O_{H2O}$ range: -6.5 to -3.8‰, SM Table 2 and Fig. 8b), and from -1.8‰ to +0.8‰ in the group of groundwater that underwent isotopic exchange with CO_2 ($\delta^{18}O_{H2O}$ range: -10.5 to -9.0‰, SM Table 2 and Fig. 8c). In Figure 8a, two groundwater samples in the Northern area showed $\delta^{18}O_{NO3}$ inside the theoretical value of $\delta^{18}O_{NO3}$ derived from nitrification of nitrogen compounds. The source of NO_3^- in sample A45 (3.5 mg/L NO_3^-, SM Table 1) could be attributed to nitrification of NH_4^+ contained in the soil, thus representing a naturally derived NO_3^-. The isotopic values measured in A28 (52 mg/L NO_3^-, SM Table 1) could be attributed to nitrification processes at manure/sewage sources, although volatilization of NH_4^+ in fertilizers resulting in a $\delta^{15}N$ increase of the residual NH_4^+ cannot be excluded (Lasagna and De Luca, 2019).

In the Southern area, the groundwater A9 is the only one falling in the field of NO_3^- fertilizers (Fig. 8b). The low concentration of NO_3^- (1 mg/L, SM Table 2) observed at this site appears in contrast with NO_3^- contamination from fertilizers. Results of the RAS monitoring at A9 showed significant temporal variations: high EC and NO_3^- (mean values of 0.98 mS/cm and 75 mg/L, respectively) were observed in the period 2011 to 2016, thereafter EC and NO_3^- decreased (mean values of 0.34 mS/cm and <0.8 mg/L, respectively). Values observed in this study (SM Table 2) suggest dilution by rainwater at the A9 site.

Many groundwater samples in Figure 8c showed isotopic compositions out of the theoretical fields of NO_3^- sources, suggesting that biogeochemical processes and/or mixing among two or more NO_3^- sources might have occurred at variable degree to account for the measured NO_3^- concentrations, and the shifting of the measured isotopic values (Xue et al., 2009; Archana et al. 2018).

Denitrification is a microbial mediated process resulting in a natural attenuation of NO_3^- concentration in water systems. If denitrification occurs, the residual NO_3^- becomes enriched in heavy isotopes, and $\delta^{15}N_{NO3}$ and $\delta^{18}O_{NO3}$ values should follow a positive linear relationship with a $\delta^{18}O_{NO3}/\delta^{15}N_{NO3}$ ratio ranging from 1:1 to 1:2 (Bottcher et al., 1990; Fukada et al., 2003). Trends observed in Figure 8 indicate that denitrification might have occurred at different degrees. The isotopic compositions of groundwater samples A2, A10, A13, A18, A20 and A58 located in the Southern area having NO_3^- concentrations in the range of 1.0 to 16 mg/L (SM Table 2) indicate that denitrification likely affected these groundwater samples in different proportions, as suggested by the positive correlation line with a slope of 0.52 (Fig. 8b).

Some groundwater samples falling in the potential denitrification area showed relatively high NO_3^- concentrations, which is apparently in contrast with the expected denitrification effect. In particular, the high enrichment in heavy isotopes in groundwater samples A25 (36 mg/L NO_3^-, Table 1) in the Northern area (Fig. 8a), A22 (76 mg/L NO_3^-, SM Table 2) in the Southern area (Fig. 8b) might be due to a high degree of denitrification, probably associated with initially high NO_3^- concentrations. However, the $\delta^{15}N_{NO3}$ and $\delta^{18}O_{NO3}$ enrichment observed in these groundwater samples might also result from the mixing of NO_3^- fertilizers with manure/sewage sources and subsequent denitrification. Mixing might have also occurred at other sites, such as A 39 (Fig. 8a) and A60 (Fig. 8c) where nitrate concentrations and isotopic signatures can be explained by a source from NO_3^- fertilizers probably mixed with manure/sewage.

Concentrations of dissolved oxygen (DO) in groundwater can be used to assess potential denitrification conditions. At DO levels above 4 mg/L, the aerobic environment would suppress denitrification, with O_2 becoming the first electron donor in place of NO_3^- (Rivett et al., 2008). Values of DO in the groundwater range from 2.9 to 9.6 mg/L in the Northern area (SM Table 1) and from 2.0 to 8.9 mg/L in the Southern area (SM Table 2), with average and SD of 6.9 ± 1.7 mg/L and 6.3 ± 1.9 mg/L, respectively. Figure 9 shows the relationship between NO_3^- and DO in the studied groundwater samples. Relatively high concentrations of NO_3^- were associated with either above or below 4 mg/L DO (Fig. 9). Concentrations of DO in most of the studied groundwater appeared unsuitable to promote denitrification. Nevertheless, the A33, A37 and A40

samples in the Northern area, and A2, A3, A9, A10, A11, A13, A18, A20 and A58 in the Southern area showed relatively low NO_3^- concentrations (below 16 mg/L), probably due to denitrification processes as suggested by the NO_3^- isotopic signatures (Fig. 8). This would be in agreement with literature reporting that denitrification may occur in micro-anaerobic parts of the aquifer where DO has been consumed (Koba et al., 1997; Moncaster et al., 2000; Wu et al., 2018).

Further elaboration may help to assess ongoing denitrification processes in the groundwater systems. In denitrification processes a negative relationship is expected when plotting $\delta^{15}N_{NO3}$ (or $\delta^{18}O_{NO3}$) versus $\ln NO_3^-$ (Bottcher et al., 1990; Fukada et al., 2003). When effects of continuous inputs of NO_3^- are supposed not to be negligible, the denitrification effect could be highlighted by the NO_3^-/Cl^- ratio (Li et al., 2019; Kou et al., 2021). Figure 10 shows the relationships between $\ln(NO_3^-/Cl^-)$ and either $\delta^{15}N_{NO3}$ and $\delta^{18}O_{NO3}$ in groundwater samples. Significant correlation was not observed in groundwater collected in the Northern area ($R^2 < 0.1$), whereas groundwater samples in the Southern area exhibited a weak inverse correlation ($R^2 = 0.16$ for $\delta^{18}O_{NO3}$ and 0.35 for $\delta^{15}N_{NO3}$, Fig. 10). These findings would indicate that denitrification processes may occur only locally in the studied areas.

The above observations suggest that variable contributions of different NO_3^- sources in groundwater may have caused the NO_3^- contamination in both areas. The Bayesian mixing model SIAR (Parnell et al., 2013) has been used to quantify the relative contributions of potential NO_3^- sources in isotopic mixtures (Meghdadi and Javar, 2018; Zhang et al., 2018; Ren et al., 2022). In this paper, fractionation factors of 26 ‰ for $\delta^{15}N_{NO3}$ and 12 ‰ for $\delta^{18}O_{NO3}$ were assumed for the groundwater A2, A10, A13, A18, A20, A58 that likely underwent denitrification, as suggested by Divers et al. (2014); for the other groundwater samples the fractionation factor was set to 0 (Jin et al., 2020; Zhang et al., 2020; Kou et al., 2021). Results of the SIAR model are shown in Figure 11a for groundwater of the Northern area, and in Figure 11b for groundwater of the Southern area. In both areas, the highest median contribution of NO_3^- in groundwater was from organic nitrogen derived from sewage and/or manure sources. The second NO_3^- source, i.e. the median contribution of NO_3^- to groundwater from NH_4^+ fertilizers, in the Southern area was higher than that observed in the Northern area (Fig. 11a). The NO_3^- in the groundwater derived from NO_3^- fertilizers and/or the soil occurred in minor proportions in both areas.

While the $\delta^{15}N_{NO3}$ and $\delta^{18}O_{NO3}$ systematic can distinguish several NO_3^- sources, do not distinguish between manure and sewage derived NO_3^-, due to overlapping isotopic signatures. The boron isotope composition ($\delta^{11}B$) is not affected by biogeochemical transformation processes, such as natural denitrification, therefore, can be used as a conservative tracer (Widory et al., 2005) to identify the impact of wastewaters on the aquatic system and as an indicator of mixing processes. Interaction of water with the aquifer matrix may cause dissolution of B-bearing silicates, adsorption-desorption processes on clays or Fe-hydroxides, thus affecting the isotopic composition and concentration of dissolved B (Xiao et al., 2013).

Results of $\delta^{11}B$ determined in samples collected in the Northern and Southern areas are reported in SM Table 1 and SM Table 2, respectively. Values of $\delta^{11}B$ measured in groundwater showed high variations with similar ranges in the Northern (5.7 ‰ to 43 ‰) and Southern area (5.4 ‰ to 41 ‰), and the same median value (32 ‰). More than 90% of $\delta^{11}B$ values measured in groundwater were higher than +20 ‰, thus in the range reported for manure (7 ‰ to 42 ‰, Widory et al., 2005; Xiao et al., 2013). The $\delta^{11}B$ values measured in samples collected from wastewater treatment plants varied from 13 ‰ to 25 ‰ with median value of 17 ‰. The values of $\delta^{11}B$ measured in wastewaters collected in the Northern were lower (13‰ to 17‰) than $\delta^{11}B$ measured in wastewaters collected in the Southern area (15‰ to 25‰). The $\delta^{11}B$ values in wastewaters of study areas were generally higher than those reported in literature for sewage (−8 ‰ to 15 ‰, Widory et al., 2005; Xiao et al., 2013). Figure 12 reports values of $\delta^{11}B$ versus 1/B in groundwater samples, the lowest values of $\delta^{11}B$ were measured in groundwater samples A35 (Fig. 12a) and A15 (Fig. 12b), respectively collected in the Northern and Southern area. The $\delta^{11}B$ values in these samples indicate a source of B derived prevalently from sewage, which is consistent with field evidences. In fact, the sample A35 was collected about 50 m downstream of a wastewater treatment plant and the sample A15 was collected in the urban area of Cagliari, in a well probably affected by leakage of sewage from the sewer network. The sample A37 in the Northern area (Fig. 12a) and samples A4, A7, A8, A10, A17, A18, A20, A58 and A60 in the Southern area (Fig. 12b) are probably affected by discharge of wastewater. In fact, most of these sampling sites were located at (A17, A18, A20) and/or downstream of (A4, A8, A60) urban areas. Natural sources of B may be attributed to the groundwater samples having relatively low concentrations of NO_3^- and B, such as samples A33 and A40 in the Northern area (SM Table 1), and A2, A9, A10 and A11 in the Southern area (SM Table 2). Groundwater sample A51, located close to the coast in the Northern area, showed the highest $\delta^{11}B$ value of 43.0 ‰ (SM Table 1), indeed, a high value in Western Mediterranean environments. Literature values of $\delta^{11}B > 40$ ‰ were

observed in saline groundwater in arid/semi-arid regions, such as the Gaza strip (Vengosh et al., 2005), and New Mexico (Langman and Ellis, 2010), and much higher $\delta^{11}B$ values (up to 64 ‰) were determined in brines originated from evaporated seawater in Laizhou Bay, China (He et al., 2018).

Figure 13 summarizes the spatial distribution of potential NO_3^- sources estimated by the SIAR model and B isotopic signatures in groundwater samples from the Northern (Fig. 13a) and Southern (Fig. 13b) areas. Groundwater samples showing NO_3^- derived from manure and fertilizers were in flat areas where agricultural and farming are more developed. This result is consistent with the use of organic and inorganic fertilizers in cultivated zones in both areas. The higher contribution of NO_3^- from NO_3-fertilizers in the Southern area (see Fig. 5b) is also consistent with a larger diffusion of greenhouse crops in the Southern area, where the use of fertilizers is widespread.

6. Conclusion

Groundwater in two study areas (Northern and Southern) of Sardinia were investigated to assess NO_3^- contamination prior to the designation of new NVZ. Results of hydrogeochemical and stable isotopes indicate that the groundwater quality in the study areas was affected by both natural processes and anthropogenic activities. The observed geochemical facies, mainly ranging from calcium bicarbonate at low salinity to sodium chloride at increasing salinity, resulted from the interaction of water with the rock-forming minerals of aquifers, and with gas phases, especially CO_2. Concentrations of NO_3^- in groundwater occurred in a large range. The present-day background threshold values were 7 and 5 mg/L NO_3^- in groundwater of the Northern and Southern area, respectively. Concentrations above NO_3^- threshold in groundwater in both study areas were mostly originated from manure, sewage, and agricultural activities.

Results of the SIAR model showed that the manure & sewage were the predominant sources contributing a median of 50% NO_3^- in groundwater of the study areas, whereas other sources showed minor contributions. Boron isotopic signature showed the manure to be the predominant source of NO_3^- in groundwater.

Nitrification and volatilization processes might have occurred at few sites, and denitrification was likely to occur at specific sites. Geographic areas showing either a predominant process or a specific NO_3^- source were not recognized in groundwater of the studied areas. Mixing among various NO_3^- sources in different proportions might account for the measured NO_3^- concentrations and the isotopic compositions of NO_3^- in several groundwater samples of both areas. These findings may be due to point sources of NO_3^- to the aquifers. Results of this study have been used by the regional water authorities to review critical cases and identify new nitrate vulnerable zones in Sardinia, according to the European Nitrate Directive.

Declaration of competing interest

All authors declare that they have no known competing financial interests or personal relationships that could have appeared to influence the work reported in this manuscript.

Acknowledgements

This work was funded by the Regione Autonoma della Sardegna (STGRI-DSCG Agreement 2016, CIG Z1A2391704,1 Scientific Responsible R. Cidu).

References

Andersson, K.K., Hooper, A.B., 1983. O_2 and H_2O are each the source of one O in NO_2^- produced from NH_3 by Nitrosomonas: 15 N-NMR evidence. FEBS Letters 164 (2), 236-240, https://doi.org/10.1016/0014-5793(83)80292-0.

Angelone, M., Gasparini, C., Guerra, M., Lombardi, S., Pizzino, L., Quattrocchi, F., Sacchi, E., Zuppi, G.M., 2005. Fluid geochemistry of the Sardinian Rift-Campidano Graben (Sardinia, Italy): fault segmentation, seismic quiescence of geochemically 'active' faults, and new constraints for selection of CO_2 storage sites. Applied Geochemistry 20, 317–340, https://doi.org/10.1016/j.apgeochem.2004.08.008.

Aravena, R., Mayer, B., 2010. Isotopes and processes in the nitrogen and sulfur cycles. In: Aelion, M.C., H€ohener, P., Hunkeler, D., Aravena, R. (Eds.), Environmental Isotopes in Biodegradation and Bioremediation. CRC Press, pp. 201-246.

Archana, A., Thibodeau, B., Geeraert, N., Xu, M.N., Kao, S-J., Baker, D.M., 2018., Nitrogen sources and cycling revealed by dual isotopes of nitrate in a complex urbanized environment. Water Research 142, 459-470, https://doi.org/10.1016/j.watres.2018.06.004.

Biddau, R., Cidu, R., Da Pelo, S., Carletti, A., Ghiglieri, G., Pittalis, D., 2019. Source and fate of nitrate in contaminated groundwater systems: Assessing spatial and temporal variations by hydrogeochemistry and

multiple stable isotope tools. Science of the Total Environment 647, 1121–1136, https://doi.org/10.1016/j.scitotenv.2018.08.007.
Biddau, R., Cidu, R., Ghiglieri, G., Da Pelo, S., Carletti, A., Pittalis, D., 2017. Nitrate occurrence in groundwater hosted in hard-rock aquifers: estimating background values at a regional scale. Italian Journal of Geoscience 136, 113–124, https://doi.org/10.3301/IJG.2016.03.
Benaglia, T., Chauveau, D., Hunter, D. R., & Young, D. S., 2009. Mixtools: An R Package for Analyzing Mixture Models. Journal of Statistical Software, 32, 1-29. https://doi.org/10.18637/jss.v032.i06
Böttcher, J., Strebel, O., Voerkelius, S., Schmidt, H.L., 1990. Using isotope fractionation of nitrate–nitrogen and nitrate–oxygen for evaluation of microbial denitrification in sandy aquifer. Journal of Hydrology 114, 413–424, https://doi.org/10.1016/0022-1694(90)90068-9.
Cao, M., Hu, A., Gad, M., Adyari, B., Qin, D., Zhang, L., Sun, Q., Yu, C-P., 2022. Domestic wastewater causes nitrate pollution in an agricultural watershed, China. Science of the Total Environment 823, 153680, https://doi.org/10.1016/j.scitotenv.2022.153680
Carrey, R., Ballesté, E., Blanch, A.R., Lucena, F., Pons, P., López, J.M., Rull, M., Solà, J., Micola, N., Fraile, J., Garrido, T., Munné, A., Soler, A., Otero, N., 2021. Combining multi-isotopic and molecular source tracking methods to identify nitrate pollution sources in surface and groundwater. Water Research 188, 116537, https://doi.org/10.1016/j.watres.2020.116537.
Cocco, F., Funedda, A., Patacca E., Scandone, P., 2012. Preliminary note on the structural setting of the central-southern Plio-Quaternary Campidano graben (Sardinia). Rendiconti Online Socieà Geologica Italiana 22, 55–57.
Cocco, F., Funedda, A., Patacca E., Scandone, P., 2013. Plio-Pleistocene extensional tectonics in the Campidano graben (SW Sardinia, Italy): preliminary note. Rendiconti Online Società Geologica Italiana 29, 31–34.
Coplen, T.B., 2011. Guidelines and recommended terms for expression of stable-isotope-ratio and gas-ratio measurement results. Rapid Communication in Mass Spectrometry 25, 2538-2560, https://doi.org/10.1002/rcm.5129.
Craig, H., 1961. Isotopic variations in meteoric waters. Science 133 (3465), 1702–1703, DOI: 10.1126/science.133.3465.1702.
Dempster, A.P., Laird, N.M., Rubin, D.B., 1977. Maximum Likelihood from Incomplete Data via the EM Algorithm. Journal of the Royal Statistical Society. Series B (Methodological), 39, 1-38. http://www.jstor.org/stable/2984875.
Divers, M.T., Elliott, E.M., Daniel, B.J., 2014. Quantification of nitrate sources to an urban stream using dual nitrate isotopes. Environmental Science & Technology 48, 10580-10587, https://doi.org/10.1021/es404880j.
EC (European Community), 1991. Council Directive 91/676/EEC of 12 December 1991 concerning the protection of waters against pollution caused by nitrates from agricultural sources. Official Journal of the European Communities L 375/1.
EC (European Commission), 2000. Directive 2000/60/EC of the European Parliament and of the Council of 23 October 2000 establishing a framework for community action in the field of water policy. Official Journal European Communities L 327.
EC (European Commission), 2006. Council Directive 2006/118/EC, on the protection of groundwater against pollution and deterioration. Official Journal European Commission, Brussels.
EC (European Commission), 2014. Commission Directive 2014/80/EU of 20 June 2014 amending Annex II to Directive 2006/118/EC of the European Parliament and of the Council on the protection of groundwater against pollution and deterioration. Official Journal of the European Union, L 182/52, Brussels, 20 June 2014.
EC (European Commission), 2021. Report from the Commission to the Council and the European Parliament on the implementation of Council Directive 91/676/EEC concerning the protection of waters against pollution caused by nitrates from agricultural sources based on Member State reports for the period 2016–2019. Brussels, 11.10.2021.
ESRI, 2013. Environmental Systems Research Institute, Esri, 380 New York Street, Redlands, California 92373-8100, USA.
Frau, F., Cidu, R., Ghiglieri, G, Caddeo, G.A., 2020. Characterization of low‐enthalpy geothermal resources and evaluation of potential contaminants. Rendiconti Lincei. Scienze Fisiche e Naturali 31, 1055-1070, https://doi.org/10.1007/s12210-020-00950-6.

Frontalini, F., Buosi, C., Da Pelo, S., Coccioni, R., Cherchi, A., Bucci C., 2009. Benthic foraminifera as bio-indicators of trace element pollution in the heavily contaminated santa gilla lagoon (Cagliari, Italy). Marine Pollution Bulletin, 58, 858-877, https://doi.org/10.1016/j.marpolbul.2009.01.015.

Fukada, T., Hiscock, K.M., Dennis, P.F., Grischek, T., 2003. A dual isotope approach to identify denitrification in groundwater at a river-bank infiltration site. Water Research 37, 3070–3078, https://doi.org/10.1016/S0043-1354(03)00176-3.

Funedda, A., Oggiano, G., Pasci, S., 2000. The Logudoro basin: a key area for the Tertiary tectono-sedimentary evolution of North Sardinia. Bollettino della Società Geologica Italiana 119, 31–38.

Giustini, F., Brilli, M., Patera, A., 2016. Mapping oxygen stable isotopes of precipitation in Italy. Journal of Hydrology: Regional Studies 8, 162–181, https://doi.org/10.1016/j.ejrh.2016.04.001.

GURI (Gazzetta Ufficiale della Repubblica Italiana), 2006. Decreto legislativo 3 aprile 2006, n. 152 Norme in materia ambientale. Gazzetta Ufficiale della Repubblica Italiana n. 88 del 14-4-2006, suppl. ord. n. 96, Roma (in Italian).

GURI (Gazzetta Ufficiale della Repubblica Italiana), 2009. Decreto legislativo 16 marzo 2009, n. 30. Attuazione della direttiva 2006/118/CE, relativa alla protezione delle acque sotterranee dall'inquinamento e dal deterioramento. Gazzetta Ufficiale della Repubblica Italiana n. 79 del 4-4-2009, Roma (in Italian).

GURI (Gazzetta Ufficiale della Repubblica Italiana), 2016. Decreto 6 luglio 2016. Recepimento della direttiva 2014/80/UE della Commissione del 20 giugno 2014 che modifica l'allegato II della direttiva 2006/118/CE del Parlamento europeo e del Consiglio sulla protezione delle acque sotterranee dall'inquinamento e dal deterioramento. Gazzetta Ufficiale della Repubblica Italiana n. 165 del 16-7-2016, Roma (in Italian).

He, S., Li, P., Su, F., Wang, D., Ren, X., 2022. Identification and apportionment of shallow groundwater nitrate pollution in Weining Plain, northwest China, using hydrochemical indices, nitrate stable isotopes, and the new Bayesian stable isotope mixing model (MixSIAR). Environmental Pollution 298, 118852, https://doi.org/10.1016/j.envpol.2022.118852.

He, Z., Ma, C., Zhou, A., Qi, H., Liu, C., Cai, H., Zhu, H., 2018. Using hydrochemical and stable isotopic ($\delta^{2}H$, $\delta^{18}O$, $\delta^{11}B$, and $\delta^{37}Cl$) data to understand groundwater evolution in an unconsolidated aquifer system in the southern coastal area of Laizhou Bay, China. Applied Geochemistry 90, 129-141, https://doi.org/10.1016/j.apgeochem.2018.01.003.

Jin, Z., Wang, J., Chen, J., Zhang, R., Li, Y., Lu, Y., He, K., 2020. Identifying the sources of nitrate in a small watershed using $\delta^{15}N$-$\delta^{18}O$ isotopes of nitrate in the Kelan Reservoir, Guangxi, China. Agriculture, Ecosystem and Environmet 297, 106936, https://doi.org/10.1016/j.agee.2020.106936.

Kazakis, N., Matiatos, I., Ntona, M-M., Bannenberg, M., Kalaitzidou, K., Kaprara, E., Mitrakas, M., Ioannidou, A., Vargemezis, G., Voudouris, K., 2020. Origin, implications and management strategies for nitrate pollution in surface and ground waters of Anthemountas basin based on a $\delta^{15}N$-NO_3^- and $\delta^{18}O$-NO_3^- isotope approach. Science of the Total Environment 724, 138211, https://doi.org/10.1016/j.scitotenv.2020.138211.

Kim, K-H., Yun, S-T., Kim, H-K., Kim, J-W., 2015. Determination of natural backgrounds and thresholds of nitrate in South Korean groundwater using model-based statistical approaches. Journal of Geochemical Exploration 148, 196-205, https://doi.org/10.1016/j.gexplo.2014.10.001.

Koba, K., Tokuchi, N., Wada, E., Nakajima, T., Iwatsubo, G., 1997. Intermittent denitrification: the application of a ^{15}N natural abundance method to a forested ecosystem. Geochimica et Cosmochimica Acta 61 (23), 5043-5050, https://doi.org/10.1016/S0016-7037(97)00284-6.

Kou, X., Ding, J., Li, Y., Li, Q., Mao, L., Xu, C., Zheng, Q., Zhuang, S., 2021. Tracing nitrate sources in the groundwater of an intensive agricultural region. Agricultural Water Management 250,106826, https://doi.org/10.1016/j.agwat.2021.106826.

Langman, J.B., Ellis, A.S., 2010. A multi-isotope (δD, $\delta^{18}O$, $^{87}Sr/^{86}Sr$, and $\delta^{11}B$) approach for identifying saltwater intrusion and resolving groundwater evolution along the Western Caprock Escarpment of the Southern High Plains, New Mexico. Applied Geochemistry 25, 159–174, https://doi.org/10.1016/j.apgeochem.2009.11.004.

Lasagna, M., De Luca, D.A., 2019. Evaluation of sources and fate of nitrates in the western Po plain groundwater (Italy) using nitrogen and boron isotopes. Environmental Science and Pollution Research, 26, 3, 2089 – 2104. https://doi.org/10.1007/s11356-017-0792-6

Li, C., Li, S-L., Yue, F-J., Liu, J., Zhong J., Yan, Z-F., Zhang, R-C., Wang, Z-J., Xu, S., 2019. Identification of sources and transformations of nitrate in the Xijiang River using nitrate isotopes and Bayesian model. Science of the Total Environment 646, 801-810, https://doi.org/10.1016/j.scitotenv.2018.07.345.

Mameli, P., Mongelli, G., Oggiano, G., Dinelli, E., 2007. Mineralogy and geochemistry of the Nurra bauxites (Western Sardinia): constraints for the conditions of the formation and parental affinity. International Journal Earth Science 96, 887-902.

Manu, E., Afrifa, G.Y., Ansah-Narh, T., Sam, F., Loh, Y.S.A., 2022. Estimation of natural background and source identification of nitrate-nitrogen in groundwater in parts of the Bono, Ahafo and Bono East regions of Ghana. Groundwater for Sustainable Development 16, 100696.

McAleer, E.B., Coxon, C.E., Richards, K.G., Jahangir, M.M.R, Grant, J., Mellander, Per.E., 2017. Groundwater nitrate reduction versus dissolved gas production: A tale of two catchments. Science of the Total Environment 586, 372–389

Meghdadi, A., Javar, N., 2018. Quantification of spatial and seasonal variations in the proportional contribution of nitrate sources using a multi-isotope approach and Bayesian isotope mixing model. Environmental Pollution 235, 207–222, https://doi.org/10.1016/j.envpol.2017.12.078.

Menció, A., Mas-Pla, J., Otero, N., Regàs, O., Boy-Roura, M., Puig, R., Bach, J., Domènech, C., Zamorano, M., Brusi, D., Folch, A., 2016. Nitrate pollution of groundwater; all right…, but nothing else? Science of the Total Environment 539, 241-251, https://doi.org/10.1016/j.scitotenv.2015.08.151.

Moncaster, S.J., Bottrell, S.H., Tellam, J.H., Lloyd, J.W., Konhauser, K.O., 2000. Migration and attenuation of agrochemical pollutants: insights from isotopic analysis of groundwater sulphate. Journal of Contaminant Hydrology. 43, 147-163, https://doi.org/10.1016/S0169-7722(99)00104-7.

Panno, S.V., Kelly, W.R., Martinsek, A.T., Hackley, K.C., 2006. Estimating background and threshold nitrate concentrations using probability graphs. Ground Water, 44, 5, 697-709. doi: 10.1111/j.1745-6584.2006.00240.x. PMID: 16961492.

Parnell, A.C., Inger, R., Bearhop, S., Jackson, A.L., 2008. SIAR: stable isotope analysis in R. http://cran.r-project.org/web/packages/siar/index.html.

Parnell, A.C., Phillips, D.L., Bearhop, S., Semmens, B.X., Ward, E.J., Moore, J.W., Jackson, A.L., Grey, J., Kelly, D.J., Inger, R., 2013. Bayesian Stable Isotope Mixing Models. Environmetrics 24, 387-399. https://doi.org/10.1002/env.2221.

Picetti, R., Deeney, M., Pastorino, S., Miller, M.R., Shah, A., Leon, D.A., Dangour, A.D., Green, R., 2022. Nitrate and nitrite contamination in drinking water and cancer risk: A systematic review with meta-analysis. Environmental Research 210, 112988, https://doi.org/10.1016/j.envres.2022.112988

Puig, R., Soler, A., Widory, D., Mas-Pla, J., Domènech, C., Otero, N., 2017. Characterizing sources and natural attenuation of nitrate contamination in the Baix Ter aquifer system (NE Spain) using a multi-isotope approach. Science of the Total Environment 580, 518–532, https://doi.org/10.1016/j.scitotenv.2016.11.206.

R Development Core Team, 2013. R: A Language and Environment for Statistical Computing. R Foundation for Statistical Computing, Vienna, Austria http://www.Rproject.org/.

RAS (Regione Autonoma della Sardegna), 2011. Caratterizzazione, obiettivi e monitoraggio dei corpi idrici sotterranei della Sardegna approvato con Deliberazione della Giunta Regionale n. 1/16 del 14/01/2011, allegato al Piano di gestione del Distretto Idrografico. Regione Autonoma della Sardegna, Cagliari (in Italian). https://www.regione.sardegna.it/documenti/1_328_20130906131252.zip

RAS (Regione Autonoma della Sardegna), 2013a. Carta geologica di base della Sardegna in scala 1:25000. Regione Autonoma della Sardegna, Cagliari.
http://www.sardegnageoportale.it/argomenti/cartageologica.html (Last accessed in January 2022).

RAS (Regione Autonoma della Sardegna), 2013b. Carta dell'Uso del Suolo in scala 1:25.000. http://www.sardegnageoportale.it/argomenti/cartedelsuolo.html (Last accessed in January 2022).

Ren, K., Pan, X. Yuan, D., Zeng, J., Liang, J., Peng, C., 2022. Nitrate sources and nitrogen dynamics in a karst aquifer with mixed nitrogen inputs (Southwest China): Revealed by multiple stable isotopic and hydro-chemical proxies. Water Research 210, 118000, https://doi.org/10.1016/j.watres.2021.118000.

Rivett, M.O., Buss, S.R., Morgan, P., Smith, J.W.N., Bemment, C.D., 2008. Nitrate attenuation in groundwater: A review of biogeochemical controlling processes. Water Research 42, 4215–4232, https://doi.org/10.1016/j.watres.2008.07.020.

Ryu, H-D., Kim, S-J., Baek, U-i., Kim, D-W., Lee, H-J., Chung, E.G., Kim, M-S., Kim, K., Lee, J.K., 2021. Identifying nitrogen sources in intensive livestock farming watershed with swine excreta treatment facility using dual ammonium ($\delta^{15}N_{NH4}$) and nitrate ($\delta^{15}N_{NO3}$) nitrogen isotope ratios axes. Science of the Total Environment 779, 146480, https://doi.org/10.1016/j.scitotenv.2021.146480.

Sarkar, S., Mukherjee, A., Duttagupta, S., Bhanja, S.N., Bhattacharya, A., Chakraborty, S., 2021. Vulnerability of groundwater from elevated nitrate pollution across India: Insights from spatio-temporal patterns using

large-scale monitoring data. Journal of Contaminant Hydrology 243, 103895, https://doi.org/10.1016/j.jconhyd.2021.103895

Sinisi, R., Mameli, P., Mongelli, G., Oggiano, G., 2012. Different Mn-ores in a continental arc setting: Geochemical and mineralogical evidences from Tertiary deposits of Sardinia (Italy). Ore Geology Reviews 47, 110–125, https://doi.org/10.1016/j.oregeorev.2012.03.006.

Stumm, W., Morgan, J.J., 1996. Aquatic chemistry, chemical equilibria and rates in natural waters. Third Edition, John Wiley & Sons Inc., New York.--pp

Torres-Martinez, J.A., Mora, A., Mahlknecht, J., Daessle, L.W., Cervantes-Aviles, P.A., Ledesma-Ruiz, R., 2021. Estimation of nitrate pollution sources and transformations in groundwater of an intensive livestock-agricultural area (Comarca Lagunera), combining major ions, stable isotopes and MixSIAR model. Environmental Pollution, 269.

Vengosh, A., Kloppmann, W., Marei, A., Livshitz, Y., Gutierrez, A., Banna, M., Guerrot, C., Pankratov, I., Raanan, H., 2005. Sources of salinity and boron in the Gaza strip: Natural contaminant flow in the southern Mediterranean coastal aquifer. Water Resources Research 41 (1), W01013, https://doi.org/10.1029/2004WR003344.

Venturi, S., Vaselli, O., Tassi, F., Nisi, B., Pennisi, M., Cabassi, J., Bicocchi, G., Rossato, L., 2015. Geochemical and isotopic evidences for a severe anthropogenic boron contamination: a case study from Castelluccio (Arezzo, central Italy). Applied Geochemistry 63, 146–157, https://doi.org/10.1016/j.apgeochem.2015.08.008.

WHO (World Health Organization), 2011. Nitrate and Nitrite in Drinking Water. Background Document for Development of WHO Guidelines for Drinking Water Quality. WHO/SDE/WSH/07.01/16/Rev/1, Geneva, p. 31.

Widory, D., Petelet-Giraud, E., Négrel, P., Ladouche, B., 2005. Tracking the sources of nitrates in groundwater using coupled nitrogen and boron isotopes: a synthesis. Environmental Science and Technology 39 (2), 539-548.

Wu, Y., Xu, L., Wang, S., Wang, Z., Shang, J., Li, X., Zheng, C., 2018. Nitrate attenuation in low-permeability sediments based on isotopic and microbial analyses. Science of the Total Environment 618, 15–25, https://doi.org/10.1016/j.scitotenv.2017.11.039.

Xiao, J., Xiao, Y.K., Jin, Z.D., He, M.Y., Liu, C.Q., 2013. Boron isotope variations and its geochemical application in nature. Australian Journal of Earth Science 60 (4), 431–447, https://doi.org/10.1080/08120099.2013.813585.

Xue, D., Botte, J., De Baets, B., Accoe, F., Nestler, A., Taylor, P., Van Cleemput, O., Berglund, M., Boeckx, P., 2009. Present limitations and future prospects of stable isotope methods for nitrate source identification in surface- and groundwater. Water Research 43, 1159–1170, https://doi.org/10.1016/j.watres.2008.12.048.

Yu, L., Zheng, T., Zheng, X., Hao, Y., Yuan, R., 2020. Nitrate source apportionment in groundwater using Bayesian isotope mixing model based on nitrogen isotope fractionation. Science of the Total Environment 718, 137242, https://doi.org/10.1016/j.scitotenv.2020.137242.

Zhang, Q., Wang, H., Wang, L., 2018. Tracing nitrate pollution sources and transformations in the over-exploited groundwater region of north China using stable isotopes. Journal of Contaminant Hydrology 218, 1–9, https://doi.org/10.1016/j.jconhyd.2018.06.001.

Zhang, H., Xu, Y., Cheng, S., Li, Q., Yu, H., 2020. Application of the dual-isotope approach and Bayesian isotope mixing model to identify nitrate in groundwater of a multiple land-use area in Chengdu Plain, China. Science of the Total Environment 717, 137134.

Captions

Figure 1. Schematic geology of Sardinia (modified by RAS, 2013a), location of study areas, water sampling sites and groundwater bodies (CIS).

Figure 2. Piper diagrams showing the relative proportions of major ions in groundwater samples collected in the Northern (a) and Southern (b) areas.

Figure 3. Cumulative distribution plots comparing NO_3^- concentrations in groundwater samples of the studied areas.

Figure 4. Statistical distributions of log-transformed NO_3^- concentration in groundwater of the Northern (a) and Southern (b) area, and values of natural NO_3^- threshold estimated on the population having the lowest NO_3^- values (shown in green).

Figure 5. Spatial distribution of NO_3^- concentrations in groundwater from the Northern (a) and Southern (b) area, superimposed on the simplified soil use map (modified after RAS, 2013b) and boxplot of the NO_3^- concentrations.

Figure 6. Relationship between the δ^2H and $\delta^{18}O$ values in groundwater of the Northern (a) and Southern (b) area. GMWL is the Global Meteoric Water Line (Craig, 1961), IMWL represents the meteoric water line proposed for southern Italy (Giustini et al., 2016). Groundwater samples within the dashed line show a negative $\delta^{18}O$ shift likely indicating oxygen isotopic exchange between groundwater and carbon dioxide.

Figure 7. Plot $\delta^{18}O_{SO4}$ versus $\delta^{34}S$ values of sulfate for groundwater samples in the Northern (a) and Southern (b) areas. The boxes show potential sulfate sources derived from Puig et al. (2017).

Figure 8. Plot $\delta^{18}O_{NO3}$ versus $\delta^{15}N$ values of nitrate for groundwater samples in the Northern (a) and Southern (b, c) area. The boxes show potential nitrate sources, with $\delta^{15}N$ values were derived from literature (Xue et al., 2009); the local $\delta^{18}O_{NO3}$ values were calculated according to Andersson and Hooper, (1983). The dashed black lines indicate typical expected slopes for denitrification processes (Böttcher et al., 1990; Fukada et al., 2003). The red line shows the linear regression of the samples having low NO_3^- concentrations due to denitrification.

Figure 9. Concentrations of NO_3^- plotted against the dissolved oxygen values in groundwater samples. The gray area indicates favorable conditions for denitrification (McAleer et al., 2017).

Figure 10. Plots $\delta^{15}N_{NO3}$ (a) and $\delta^{18}O_{NO3}$ (b) versus $\ln(NO_3^-/Cl^-)$ in the studied groundwater samples.

Figure 11. Proportional contributions of the main potential nitrate sources in the Northern (a) and Southern (b) areas estimated by the SIAR model. The 25th, 50th, and 75th percentiles are shown in each box, and the lower and upper whiskers indicate the 5th and 95th percentiles, respectively, and circles are the outliers.

Figure 12. Values of $\delta^{11}B$ versus 1/B for groundwater samples in the Northern (a) and Southern (b) areas, showing potential sources B in the groundwater and wastewater samples. Ranges of the potential B sources were derived from literature (Widory et al., 2005; Xiao et al., 2013).

Figure 13. Spatial distribution of the potential NO_3^- sources estimated by isotopic analyses and the SIAR model in groundwater samples from the Northern (a) and Southern (b) areas, together with the simplified soil use map (modified after RAS, 2013b).

Supplementary Material Table 1. Physical-chemical parameters, inorganic components and stable isotope ratios in water samples collected in the Northern area. GW = groundwater; WW = wastewater; sd = standard deviation

Supplementary Material Table 2. Physical-chemical parameters, inorganic components and stable isotope ratios in water samples collected in the Southern area. GW = groundwater; WW = wastewater; sd = standard deviation.

Graphical Abstract

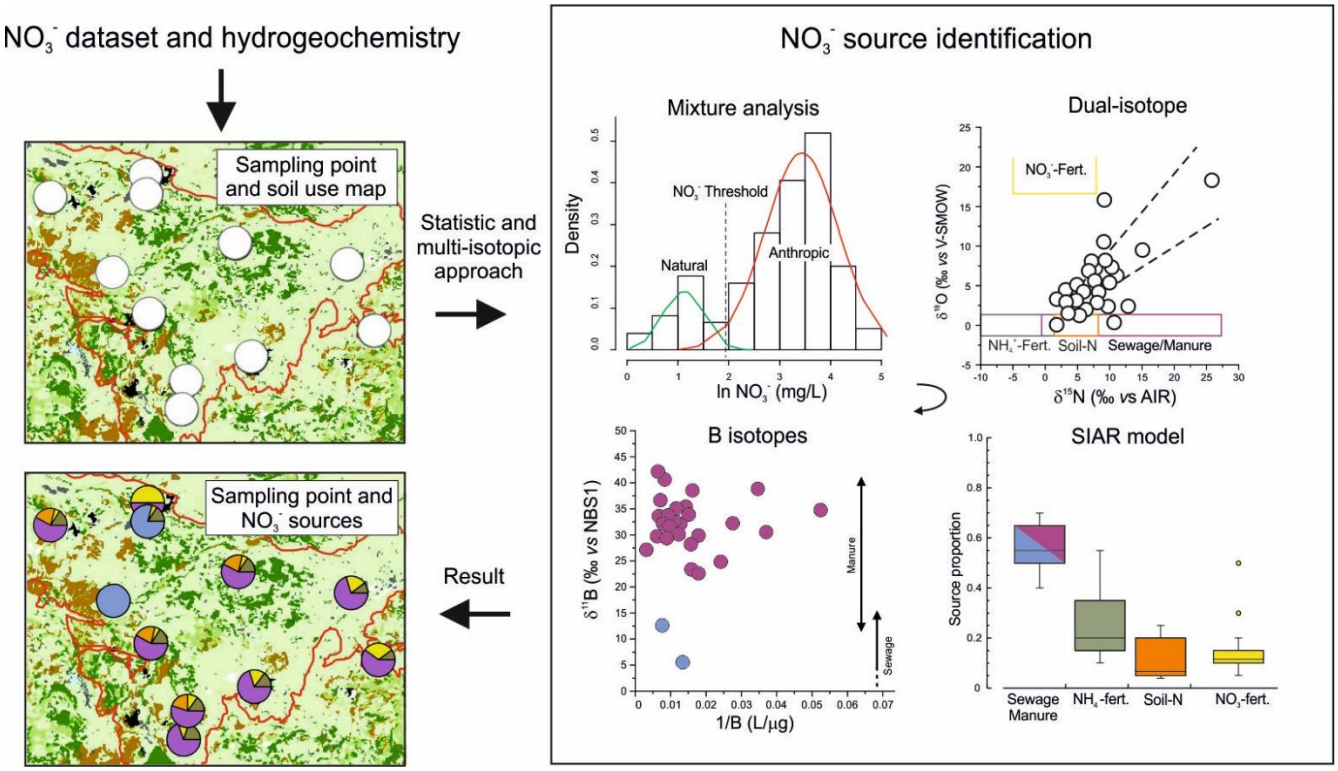

Figure 1

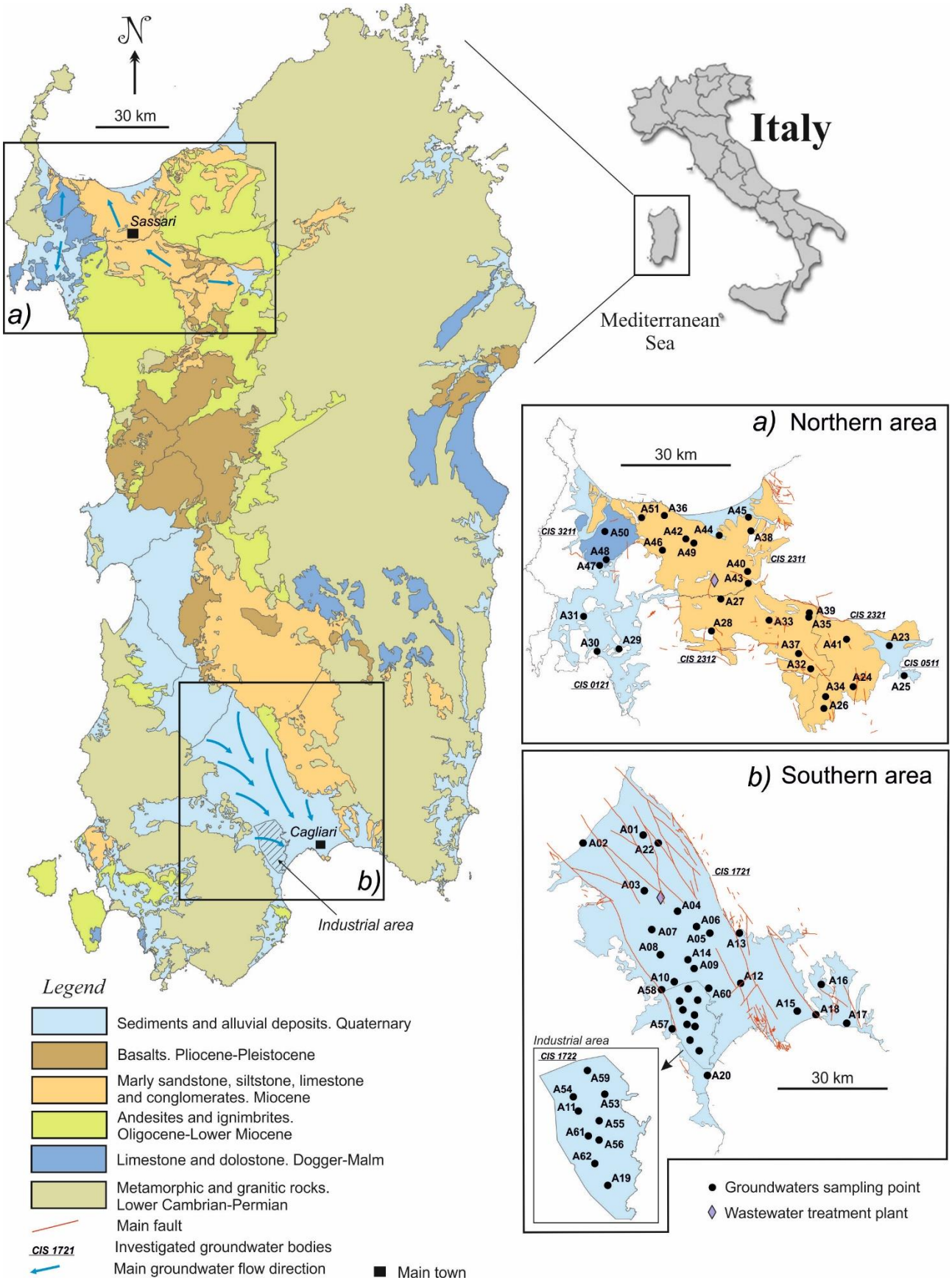
N
30 km
Sassari
a)
Cagliari
b)
Industrial area
Italy
Mediterranean Sea
a) Northern area
30 km
CIS 3211
CIS 2311
CIS 2321
CIS 2312
CIS 0121
CIS 0511
b) Southern area
CIS 1721
Industrial area
CIS 1722
30 km
Legend
Sediments and alluvial deposits. Quaternary
Basalts. Pliocene-Pleistocene
Marly sandstone, siltstone, limestone and conglomerates. Miocene
Andesites and ignimbrites. Oligocene-Lower Miocene
Limestone and dolostone. Dogger-Malm
Metamorphic and granitic rocks. Lower Cambrian-Permian
Main fault
CIS 1721 Investigated groundwater bodies
Main groundwater flow direction
Main town
Groundwaters sampling point
Wastewater treatment plant

Figure 2

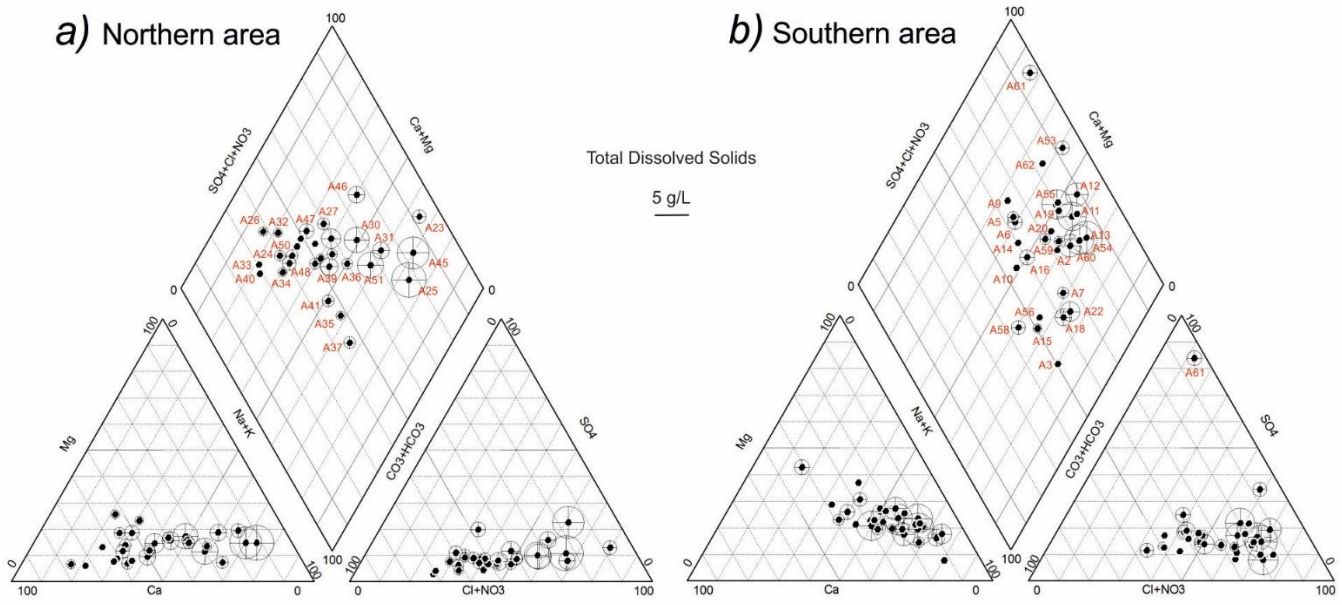
a) Northern area
b) Southern area
Total Dissolved Solids
5 g/L
SO4+Cl+NO3
Ca+Mg
Na+K
CO3+HCO3
Mg
Ca
Cl+NO3
SO4
100
0

Figure 3

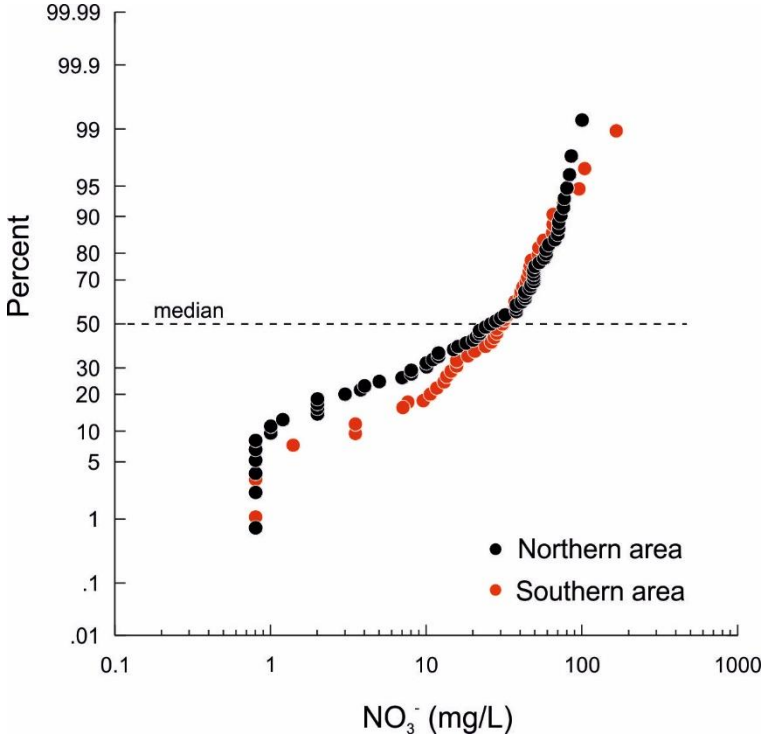
99.99
99.9
99
95
90
80
70
50
30
20
10
5
1
.1
.01
Percent
median
Northern area
Southern area
0.1
1
10
100
1000
NO3- (mg/L)

Figure 4

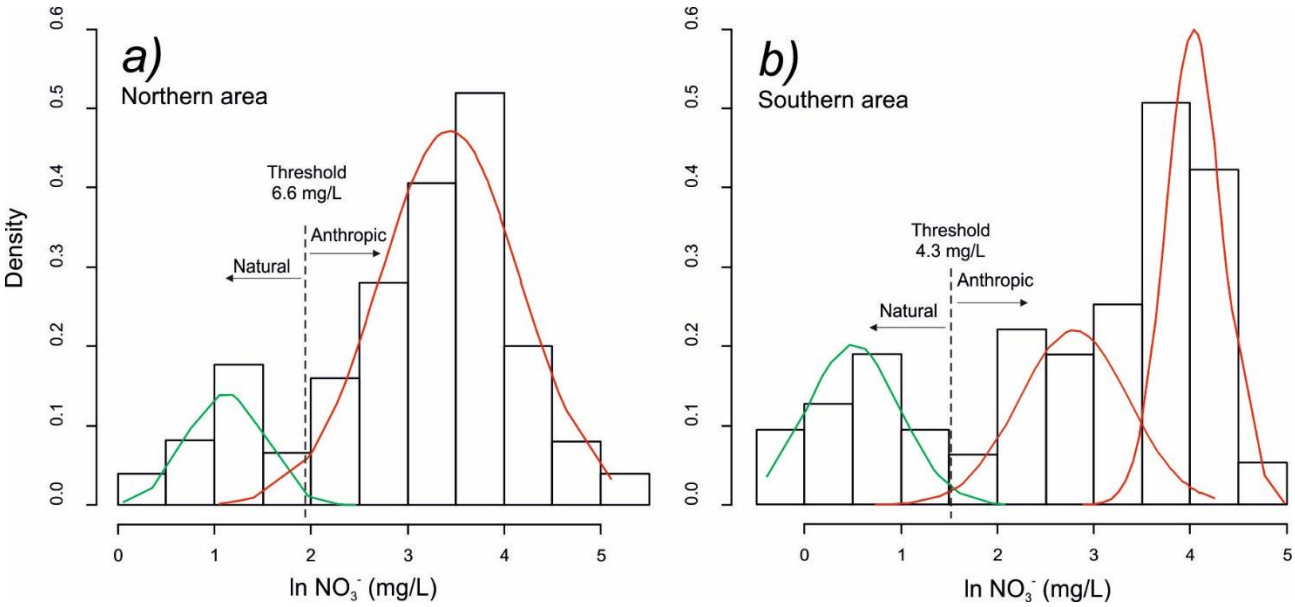
a)
Northern area
Threshold
6.6 mg/L
Anthropic
Natural
Density
0.0
0.1
0.2
0.3
0.4
0.5
0.6
0
1
2
3
4
5
ln NO3- (mg/L)
b)
Southern area
Threshold
4.3 mg/L
Anthropic
Natural
ln NO3- (mg/L)

Figure 5

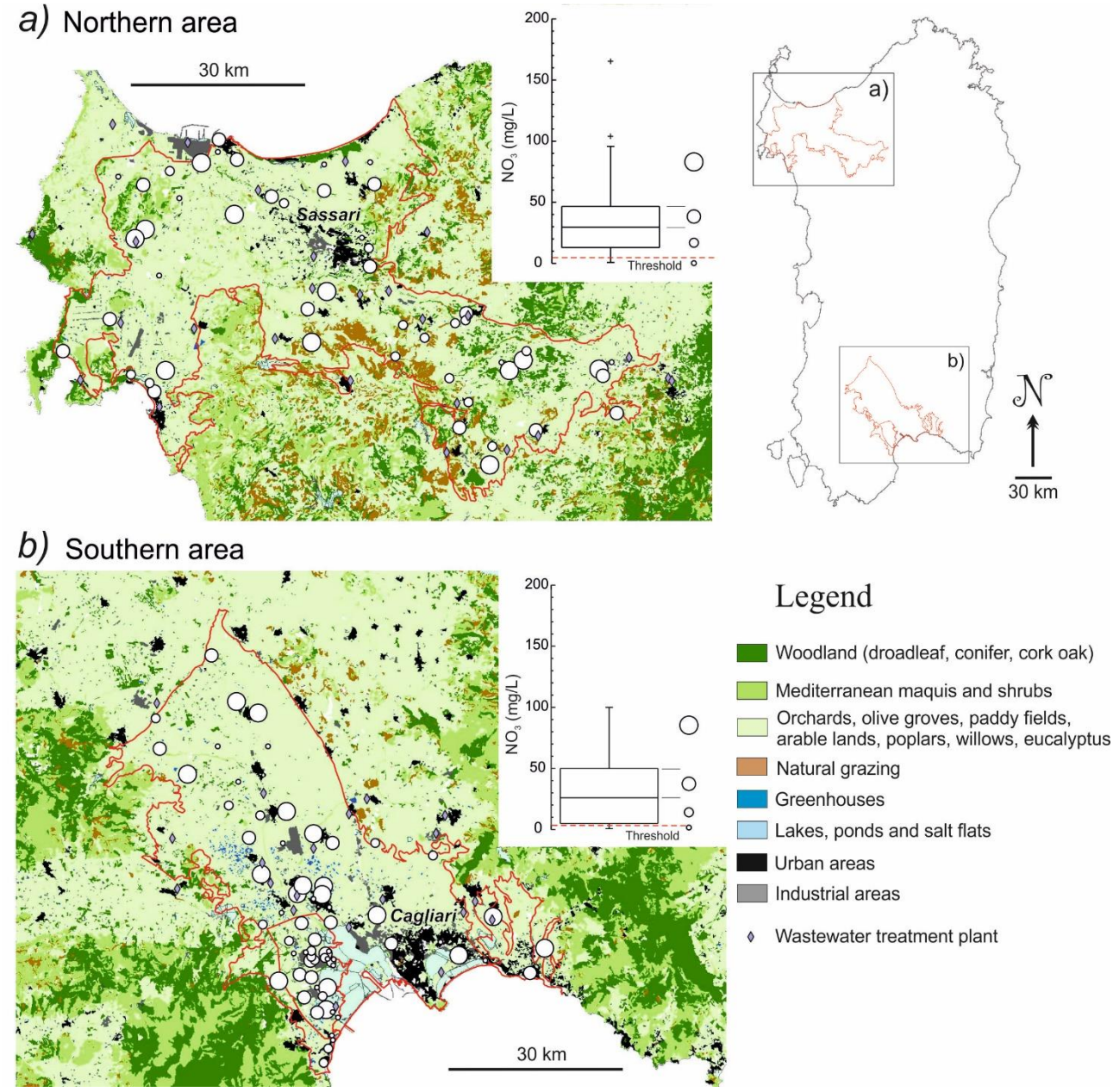
a) Northern area
30 km
Sassari
200
150
100
50
0
NO3 (mg/L)
Threshold
a)
b)
N
30 km
b) Southern area
Cagliari
30 km
Legend
Woodland (droadleaf, conifer, cork oak)
Mediterranean maquis and shrubs
Orchards, olive groves, paddy fields, arable lands, poplars, willows, eucalyptus
Natural grazing
Greenhouses
Lakes, ponds and salt flats
Urban areas
Industrial areas
Wastewater treatment plant

Figure 6

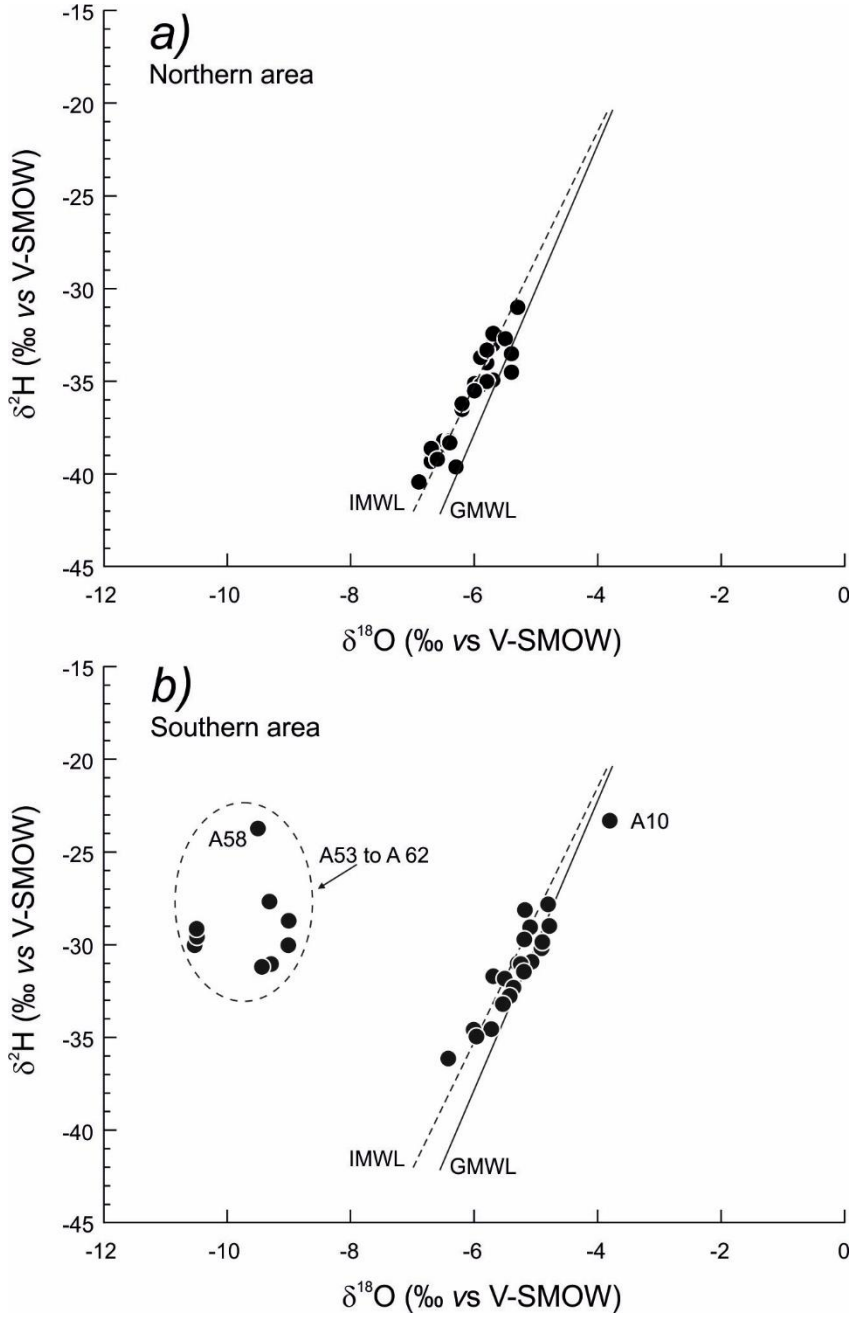
a)
Northern area
IMWL
GMWL
δ²H (‰ vs V-SMOW)
δ¹⁸O (‰ vs V-SMOW)
b)
Southern area
A58
A53 to A 62
A10
IMWL
GMWL
δ²H (‰ vs V-SMOW)
δ¹⁸O (‰ vs V-SMOW)

Figure 7

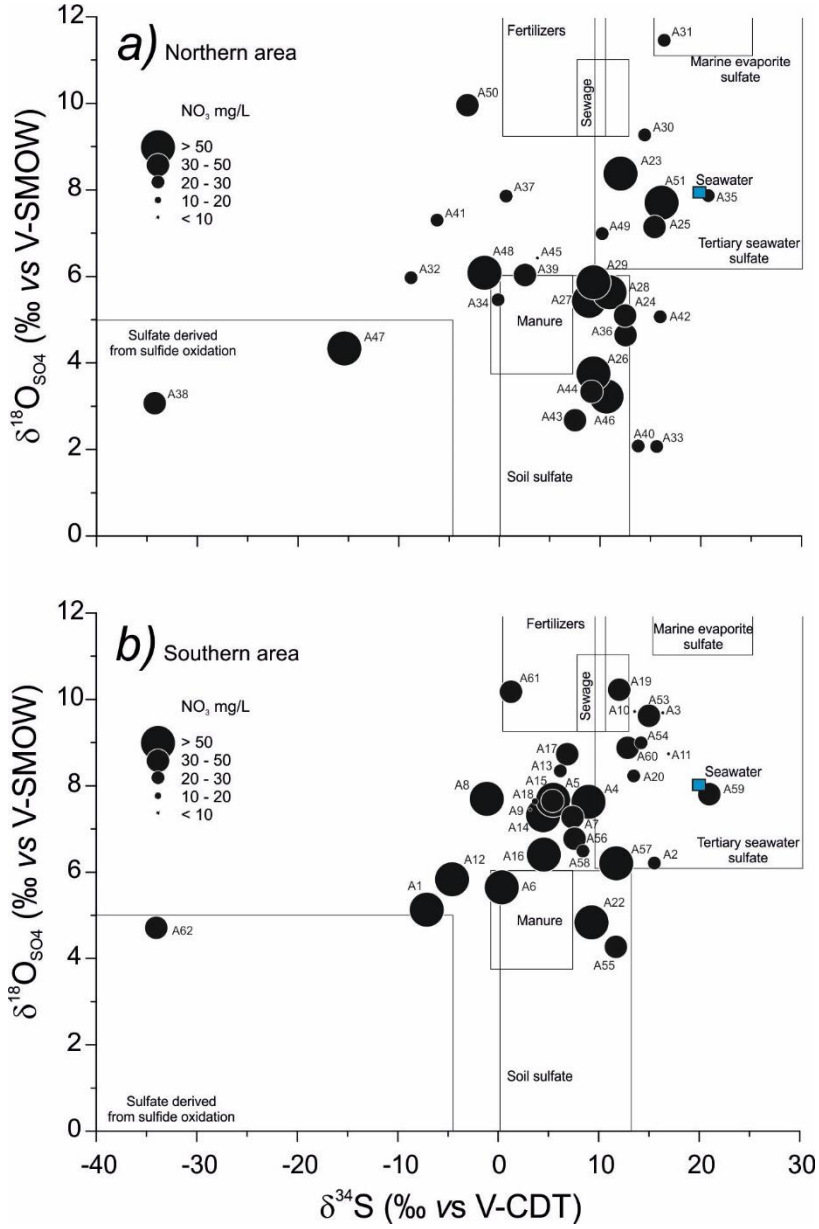
a) Northern area
NO3 mg/L
> 50
30 - 50
20 - 30
10 - 20
< 10
Fertilizers
Sewage
Marine evaporite sulfate
Seawater
Tertiary seawater sulfate
Manure
Soil sulfate
Sulfate derived from sulfide oxidation
b) Southern area
δ18OSO4 (‰ vs V-SMOW)
δ34S (‰ vs V-CDT)

Figure 8

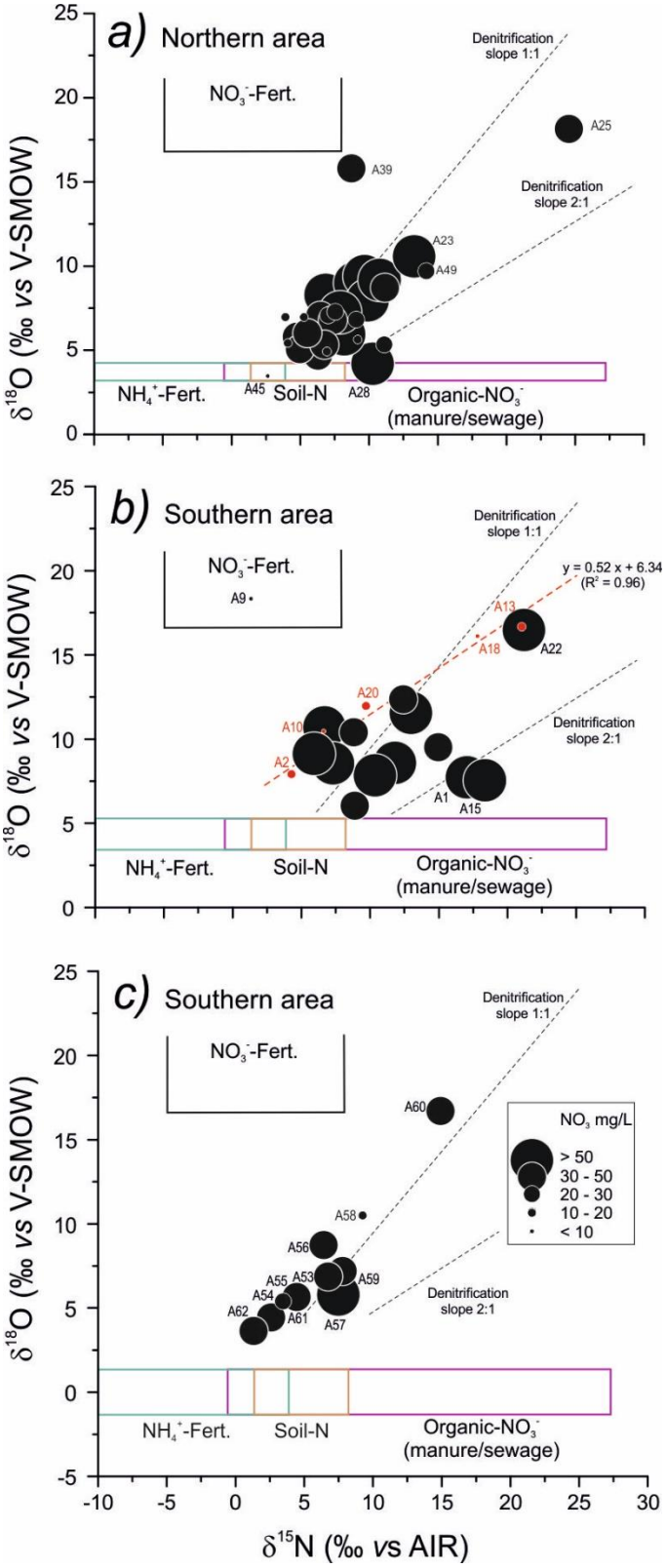
a) Northern area
Denitrification slope 1:1
NO3-Fert.
A25
A39
Denitrification slope 2:1
A23
A49
NH4+-Fert.
A45
Soil-N
A28
Organic-NO3- (manure/sewage)
δ18O (‰ vs V-SMOW)
b) Southern area
Denitrification slope 1:1
NO3-Fert.
A9
y = 0.52 x + 6.34
(R2 = 0.96)
A13
A18
A22
A20
A10
A2
Denitrification slope 2:1
A1
A15
NH4+-Fert.
Soil-N
Organic-NO3- (manure/sewage)
δ18O (‰ vs V-SMOW)
c) Southern area
Denitrification slope 1:1
NO3-Fert.
A60
NO3 mg/L
> 50
30 - 50
20 - 30
10 - 20
< 10
A58
A56
A55
A53
A59
A54
A62
A61
A57
Denitrification slope 2:1
NH4+-Fert.
Soil-N
Organic-NO3- (manure/sewage)
δ18O (‰ vs V-SMOW)
δ15N (‰ vs AIR)

Figure 9

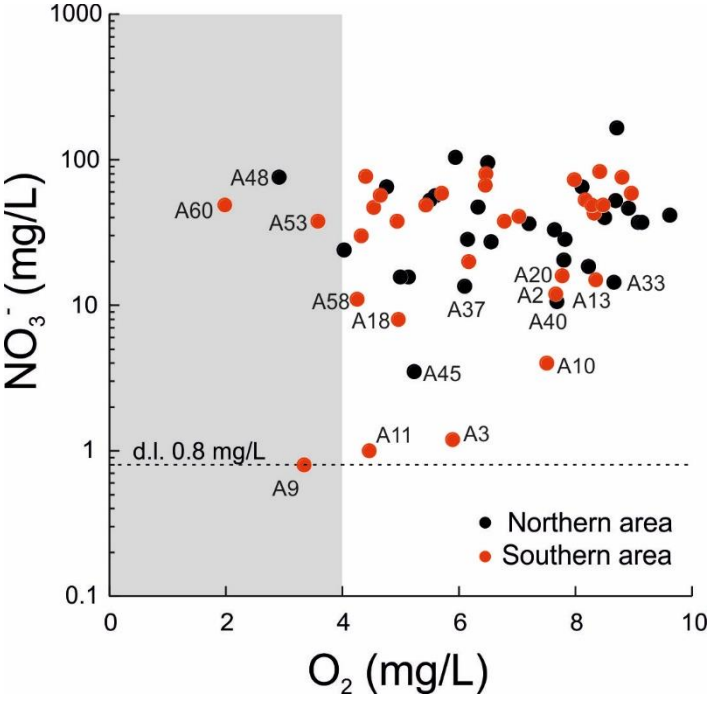
1000
100
10
1
0.1
NO_3^- (mg/L)
0
2
4
6
8
10
O_2 (mg/L)
d.l. 0.8 mg/L
A48
A60
A53
A58
A18
A37
A20
A2
A13
A33
A40
A45
A10
A11
A3
A9
Northern area
Southern area

Figure 10

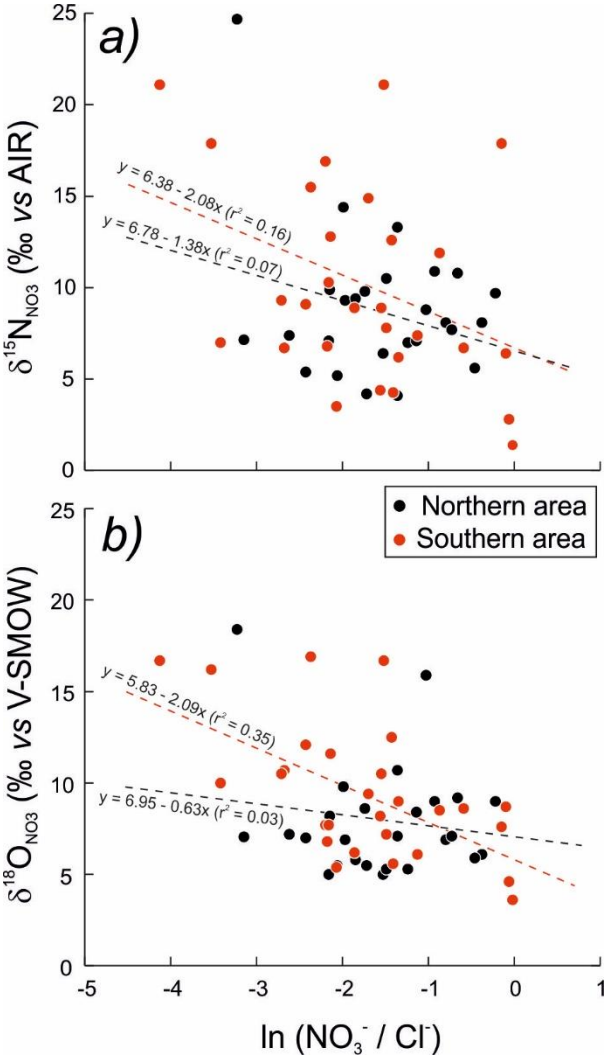
a)
b)
Northern area
Southern area
y = 6.38 - 2.08x (r² = 0.16)
y = 6.78 - 1.38x (r² = 0.07)
y = 5.83 - 2.09x (r² = 0.35)
y = 6.95 - 0.63x (r² = 0.03)
δ15NNO3 (‰ vs AIR)
δ18ONO3 (‰ vs V-SMOW)
ln (NO3- / Cl-)

Figure 11

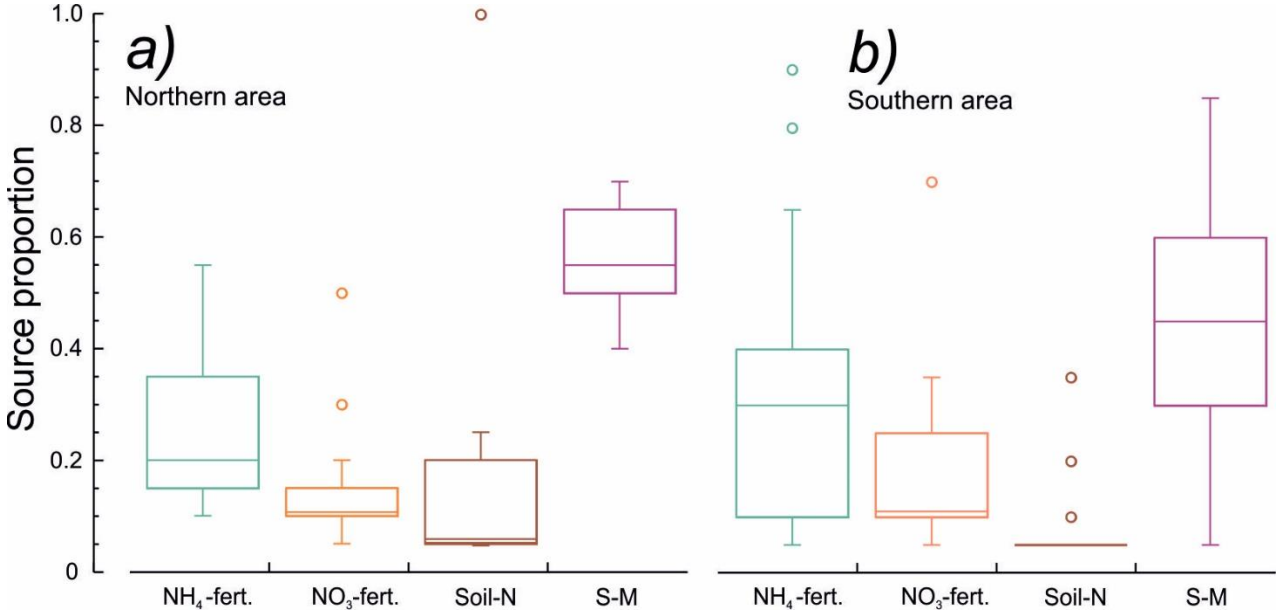
a)
Northern area
b)
Southern area
Source proportion
1.0
0.8
0.6
0.4
0.2
0
NH4-fert.
NO3-fert.
Soil-N
S-M
NH4-fert.
NO3-fert.
Soil-N
S-M

Figure 12

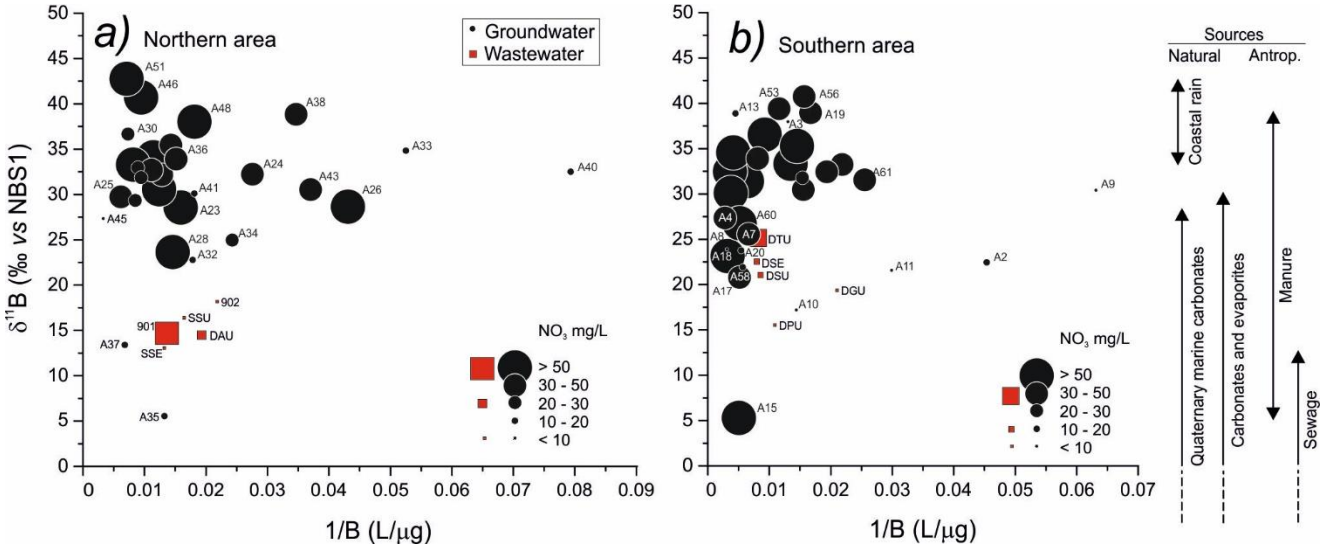
a) Northern area
Groundwater
Wastewater
δ11B (‰ vs NBS1)
1/B (L/μg)
NO3 mg/L
> 50
30 - 50
20 - 30
10 - 20
< 10
A51
A46
A48
A38
A30
A36
A33
A40
A24
A43
A26
A25
A41
A23
A45
A28
A34
A32
902
SSU
901
DAU
A37
SSE
A35
b) Southern area
A53
A56
A13
A19
A61
A9
A4
A60
A7
DTU
A8
A20
A18
DSE
A58
DSU
A17
A11
A2
DGU
A10
DPU
A15
Sources
Natural
Antrop.
Coastal rain
Quaternary marine carbonates
Carbonates and evaporites
Manure
Sewage

Figure 13

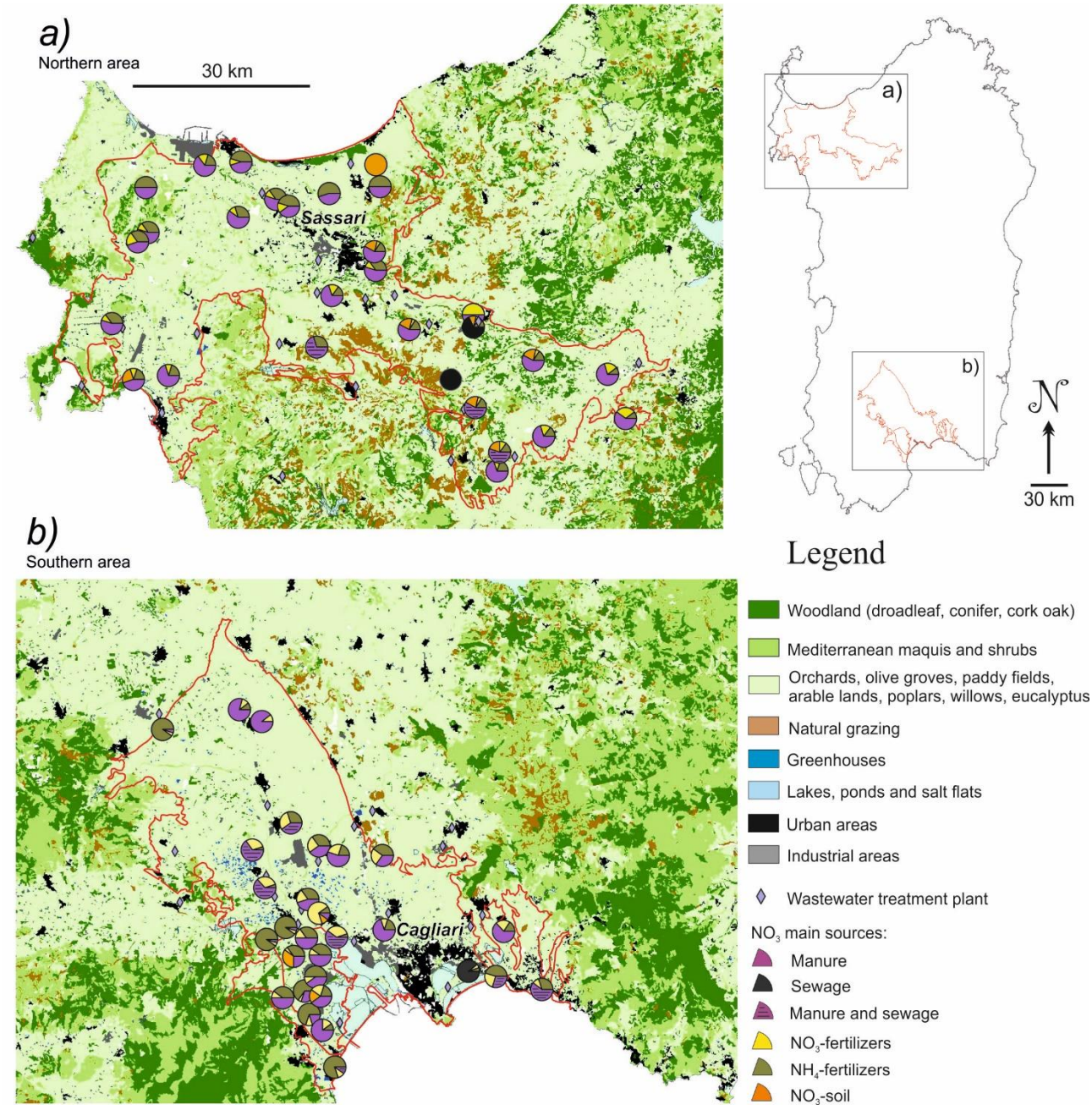
a)
Northern area
30 km
Sassari
b)
Southern area
Cagliari
a)
b)
N
30 km
Legend
Woodland (droadleaf, conifer, cork oak)
Mediterranean maquis and shrubs
Orchards, olive groves, paddy fields, arable lands, poplars, willows, eucalyptus
Natural grazing
Greenhouses
Lakes, ponds and salt flats
Urban areas
Industrial areas
Wastewater treatment plant
NO3 main sources:
Manure
Sewage
Manure and sewage
NO3-fertilizers
NH4-fertilizers
NO3-soil

Electronic Supplementary Material (for online publication only)

Supplementary Material Table 2.xlsx